

# Constraints on the inflaton potential from scalar-induced gravitational waves and primordial black holes

Shi-Jie Wang,<sup>a</sup> Nan Li<sup>a,1</sup>

<sup>a</sup>Department of Physics, College of Sciences, Northeastern University, Shenyang, 110819, China

E-mail: [2300203@stu.neu.edu.cn](mailto:2300203@stu.neu.edu.cn), [linan@mail.neu.edu.cn](mailto:linan@mail.neu.edu.cn)

**Abstract.** A plateau on the background inflaton potential  $V_b(\phi)$  can lead cosmic inflation into an ultraslow-roll phase, greatly enhancing the primordial power spectrum on small scales, and resulting in intensive scalar-induced gravitational waves (GWs) and abundant primordial black holes (PBHs). In this work, we construct an anti-symmetric perturbation  $\delta V(\phi)$  on  $V_b(\phi)$  with three model parameters, the position, width, and slope of  $\delta V(\phi)$ , and constrain these parameters from the potential stochastic gravitational wave background (SGWB) in the NANOGrav 15-year data set. The GW spectrum from the supermassive black hole binaries (SMBHBs) with two model parameters, the amplitude and spectral index, is also investigated for comparison. We perform the Bayesian analysis in three steps with increasing number of model parameters, and obtain the allowed parameter ranges. When the constraints on PBH abundance are taken into account, these ranges become further narrower. We find that the increase of model parameters cannot significantly improve the Bayes factors, and the model with an almost perfect plateau on  $V_b(\phi)$  is favored. Moreover, the interpretation of the SGWB only via the GWs from SMBHBs is not preferred by the data. Two different forms of  $V_b(\phi)$  are considered, and the analogous results confirm the generality and robustness of our work.

**Keywords:** Scalar-induced gravitational waves, Primordial black holes, Ultraslow-roll inflation, Bayesian analysis

---

<sup>1</sup>Corresponding author.

---

## Contents

<b>1</b>	<b>Introduction</b>	<b>1</b>
<b>2</b>	<b>USR inflation and PBHs</b>	<b>3</b>
2.1	Basic equations	3
2.2	Inflaton potentials	4
2.3	Power spectra and PBH abundance	5
<b>3</b>	<b>SIGWs</b>	<b>7</b>
3.1	Basic equations	7
3.2	SIGW spectra	8
<b>4</b>	<b>Bayesian analysis</b>	<b>9</b>
4.1	Likelihood function	9
4.2	Data	10
4.3	Prior distributions and Bayes factor	11
<b>5</b>	<b>Constraints on the inflaton potential in the KKLT model</b>	<b>11</b>
5.1	Case with two model parameters	12
5.2	Case with three model parameters	12
5.3	Case with SMBHBs	16
5.4	Bayes factors	19
<b>6</b>	<b>Conclusion</b>	<b>20</b>
<b>A</b>	<b>Constraints on the inflaton potential in the Starobinsky model</b>	<b>21</b>

---

## 1 Introduction

The detections of the gravitational waves (GWs) from compact binary mergers (e.g., the black hole binaries (BHBs) [1, 2] and the neutron star binaries [3, 4]) have marked the beginning of an unprecedented multi-messenger epoch in modern cosmology. Moreover, in the early Universe, primordial GWs may also have different origins, such as cosmological phase transitions [5–8], topological defects [9–12], preheating [13, 14], kination-domination [15–18], and particle production [19, 20]. In addition, GWs can also be induced by scalar perturbations during cosmic inflation [21–25]. Altogether, these diverse sources collectively contribute to the stochastic GW background (SGWB), offering a new tool for probing the Universe and providing crucial information and insight for understanding astrophysics and cosmology beyond traditional electromagnetic methods [26, 27]. Therefore, the observation of the SGWB is the primary goal of various GW detectors that are designed for these faint but informative signals from a wide range of cosmic events.

The recent observations from the European Pulsar Timing Array (EPTA) [28, 29], Parkes PTA [30, 31], Chinese PTA [32], Meerkat PTA [33], and especially North American Nanohertz Observatory for Gravitational Waves (NANOGrav) [34–37], have provided multiple pieces of evidence for an excess of the red common-spectrum signals at low frequencies (the nHz range)

with respect to the Hellings–Downs correlations [38], supporting the potential existence of the isotropic SGWB. These signals follow a power-law spectrum, consistent with the GW spectrum from the orbital evolution of supermassive BHBs (SMBHBs) [37]. However, the spectral index deviates from the SMBHB-only model, suggesting environmental effects or other possible physical origins (e.g., cosmic (super)strings, first-order phase transitions, domain walls, large primordial fluctuations, and audible axions) [36]. These observations have aroused intensive research interests and debates in recent years [39–87]. For instance, a multi-model analysis was performed on the above-mentioned models, with and without the SMBHB background, indicating that these models are capable of fitting the NANOGrav data as well as SMBHBs alone [88]. Also, in Ref. [89], the authors combined the NANOGrav and EPTA-DR2new data sets, and found that the audible axion or string signals fit the data better than SMBHBs. These studies pointed out alternative interpretations of the PTA data beyond the SMBHB-only model, and this is also the topic of our present work.

In this work, we attribute the SGWB to the scalar-induced GWs (SIGWs), which are the second-order effect from the first-order scalar perturbations generated during inflation. If these scalar perturbations are large enough on small scales, they can also produce a significant number of primordial black holes (PBHs) at the same time [90–92]. These PBHs can explain a portion of the BHB merger events [93–96], serve as the seeds of supermassive black holes at galactic centers [97–101], and more importantly, are a natural candidate of dark matter (DM) [102–107]. For more recent researches on SIGWs and PBHs, especially in the light of the NANOGrav 15-year data set, see Refs. [108–153] and the reviews [154–157], with the references therein.

Usually, the single-field slow-roll (SR) inflation models lead to a nearly scale-invariant power spectrum of scalar perturbations, confirmed by the measurements of the cosmic microwave background (CMB) anisotropies on large scales [158]. However, the SIGWs from such a power spectrum are too weak to account for the SGWB. To have sufficiently large SIGWs, it is necessary to break the SR conditions by imposing a period of ultraslow-roll (USR) phase in cosmic inflation, during which the inflaton potential is rather flat, and the inflaton rolls down extremely slowly. In the USR stage, the SR parameters change dramatically, and the power spectrum on small scales is significantly amplified, generating intensive SIGWs and abundant PBHs simultaneously. Nevertheless, the position and duration of the USR phase must be carefully adjusted, so that it only influences the physics on small scales, without spoiling the large-scale CMB constraints. There are many mechanisms for the USR inflation, which can be realized by a inflection point or a saddle point on the inflaton potential [159–162], in modified gravity theories [163–165], or in supergravity models [166–168], etc. For a comprehension of the USR inflation and its effects on SIGWs and PBHs, see Refs. [169–192]. In this paper, following our previous works in Refs. [193–198], we consider an anti-symmetric perturbation  $\delta V(\phi)$  on the background inflaton potential to realize the USR phase.

Our goal in this work is to determine the position, width, and slope of  $\delta V(\phi)$  by the constraints from the SIGW spectrum and the PBH abundance. First, we adopt the NANOGrav 15-year data set, utilize a modified version of the **SIGWfast** code [199] to compute the SIGW spectrum, and perform Bayesian analysis [200] by the **PTArcade** code [201]. Second, the model parameters extracted from the SIGW spectrum must lead to reasonable PBH abundance in relevant mass range at the same time, and this demand will further shrink the allowed parameter space. Third, as there is also possibility that the SGWB is generated from SMBHBs [34, 36], we still need to consider the scenario that the SGWB origins from both SIGWs and SMBHBs. These three points will constitute the main body of our work. More importantly,

we do not assume any simple form of the primordial power spectrum as done in many previous literature, but constrain the model parameters of the inflaton potential directly from the GW data. This operation is also supported by Ref. [202], where the authors studied different methods (template based, agnostic, and ab initio) to constrain the USR phase, and found that using the explicit USR construction leads to the minimum residuals.

This paper is organized as follows. In Sec. 2, we introduce two different background inflaton potentials, show the power spectrum of the primordial curvature perturbation, and calculate the PBH abundance. In Sec. 3, we derive the SIGW spectrum. The NANOGrav 15-year data set and the relevant Bayesian analysis method are reviewed in Sec. 4. With all these preparations, we constrain our inflation models in Sec. 5 and App. A, with two model parameters, three model parameters, and SMBHBs taken into account, respectively. The Bayes factors between different models are also calculated and discussed in detail. We conclude in Sec. 6. We work in the natural system of units and set  $c = \hbar = k_B = 1$ .

## 2 USR inflation and PBHs

In this section, we discuss the equation of motion for the primordial curvature perturbation  $\mathcal{R}$ , introduce its power spectrum  $\mathcal{P}_{\mathcal{R}}(k)$ , and show the calculation of PBH abundance  $f_{\text{PBH}}$ .

### 2.1 Basic equations

We start from the action of the single-field inflation,

$$S = \int d^4x \sqrt{-g} \left[ \frac{m_{\text{P}}^2}{2} R - \frac{1}{2} \partial_\mu \phi \partial^\mu \phi - V(\phi) \right],$$

where  $m_{\text{P}} = 1/\sqrt{8\pi G} = 2.435 \times 10^{18}$  GeV is the reduced Planck mass,  $R$  is the Ricci scalar,  $\phi$  is the inflaton field, and  $V(\phi)$  is its potential, respectively. By variation of  $S$ , the equation of motion for  $\phi$  can be obtained as the Klein–Gordon equation,

$$\ddot{\phi} + 3H\dot{\phi} + V_{,\phi} = 0, \quad (2.1)$$

where  $H$  is Hubble expansion rate.

During inflation, it is more convenient to use the number of  $e$ -folds  $N$  to describe cosmic expansion, defined as  $dN = H(t) dt = d \ln a(t)$ , where  $t$  is the cosmic time,  $a(t)$  is the scale factor, and  $H = \dot{a}/a$ . In addition, to characterize the SR behaviors of the inflaton, two SR parameters can be introduced as

$$\varepsilon = -\frac{\dot{H}}{H^2} = \frac{\phi_{,N}^2}{2m_{\text{P}}^2}, \quad \eta = -\frac{\ddot{\phi}}{H\dot{\phi}} = \frac{\phi_{,N}^2}{2m_{\text{P}}^2} - \frac{\phi_{,NN}}{\phi_{,N}}. \quad (2.2)$$

With these parameters, Eq. (2.1) can be reexpressed as

$$\phi_{,NN} + (3 - \varepsilon)\phi_{,N} + \frac{1}{H^2}V_{,\phi} = 0,$$

and the Friedmann equation for cosmic expansion can be written as

$$H^2 = \frac{V}{(3 - \varepsilon)m_{\text{P}}^2}.$$

Then, we move on to the perturbations on the background spacetime. In Newtonian gauge, the perturbed metric reads

$$ds^2 = -(1 + 2\Psi) dt^2 + a^2(t) \left[ (1 - 2\Psi) \delta_{ij} + \frac{1}{2} h_{ij} \right] dx^i dx^j, \quad (2.3)$$

where  $\Psi$  is the first-order scalar perturbation,  $h_{ij}$  is the second-order tensor perturbation, and we have neglected the vector perturbation and anisotropic stress here. A more frequently used gauge-invariant scalar perturbation is the primordial curvature perturbation  $\mathcal{R}$ ,

$$\mathcal{R} = \Psi + \frac{H}{\dot{\phi}} \delta\phi,$$

where  $\delta\phi$  is the perturbation of the inflaton field. The equation of motion for its Fourier mode  $\mathcal{R}_k$  is the Mukhanov–Sasaki equation [203, 204],

$$\mathcal{R}_{k,NN} + (3 + \varepsilon - 2\eta) \mathcal{R}_{k,N} + \frac{k^2}{H^2 e^{2N}} \mathcal{R}_k = 0. \quad (2.4)$$

## 2.2 Inflaton potentials

The Fourier mode  $\mathcal{R}_k$  can be obtained by numerically solving Eqs. (2.1), (2.2), and (2.4), which requires us to specify the form of the inflaton potential  $V(\phi)$ . Following our previous works in Refs. [193–198], we decompose  $V(\phi)$  as the sum of its background potential  $V_b(\phi)$  and a perturbation  $\delta V(\phi)$  on it,

$$V(\phi) = V_b(\phi) + \delta V(\phi).$$

For the generality of our discussions, we explore two different background potentials in this work. The first is the Kachru–Kallosh–Linde–Trivedi (KKLT) potential [205],

$$V_b(\phi) = V_0 \frac{\phi^2}{\phi^2 + (m_P/2)^2},$$

where the parameter  $V_0$  indicates the energy scale of inflation. The second is the Starobinsky potential [206], which originates from an  $R^2$ -modification in the Einstein–Hilbert action and can be mapped to a scalar field  $\phi$  minimally coupled to gravity via a conformal transformation,

$$V_b(\phi) = V_0 \left( 1 - e^{\sqrt{2/3} \phi / m_P} \right)^2.$$

Here, we set  $V_0$  the same as that in the KKLT model, so that the inflatons roll down the potentials from the same energy scale.

Then, we parameterize the perturbation  $\delta V(\phi)$  in an anti-symmetric form as

$$\delta V(\phi) = -A(\phi - \phi_0) \exp \left[ -\frac{(\phi - \phi_0)^2}{2\sigma^2} \right], \quad (2.5)$$

where  $A$ ,  $\phi_0$ , and  $\sigma$  are three model parameters that determine the amplitude, position, and width of  $\delta V(\phi)$ , respectively. For convenience, we reexpress  $A$  as

$$A = V_{b,\phi}(\phi_0)(1 + A_0), \quad (2.6)$$

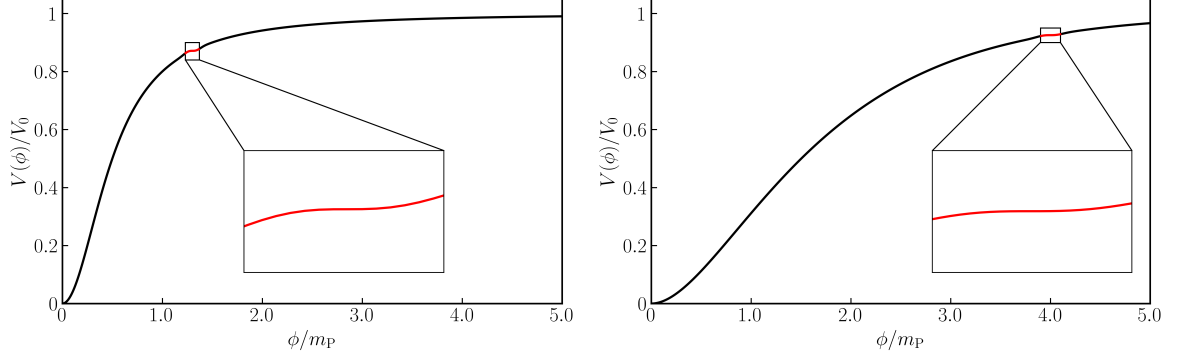


**Figure 1.** The inflaton potentials for the KKLt model (the left panel) and the Starobinsky model (the right panel), with the relevant USR regions shown in the insets. The shapes of these two potentials are similar, while the Starobinsky potential decreases relatively slowly. The inflatons roll down these two potentials from the same energy scale at  $V_0/m_P^4 = 10^{-10}$  and pass through the USR regions at different positions, resulting in abundant PBHs and intensive SIGWs.

with  $V_{b,\phi}(\phi_0) = dV_b(\phi)/d\phi|_{\phi_0}$  denoting the slope of the background potential  $V_b(\phi)$  at the position  $\phi_0$ . By this means,  $A_0$  characterizes the deviation of  $V(\phi)$  from a perfect plateau at  $\phi_0$ . We plot the two inflaton potentials in Fig. 1, with the USR regions shown in the insets.

Furthermore, in the KKLt model, we set  $V_0/m_P^4 = 10^{-10}$ ,  $\phi_i/m_P = 3.30$ , and  $\phi_{i,N}/m_P = -0.0137$  as the initial conditions for inflation, such that there can be a nearly scale-invariant power spectrum, with the spectral index  $n_s = 0.9600$  and a relatively small tensor-to-scalar ratio  $r = 0.00321$ , favored by the CMB observations on large scales [158]. Similarly, in the Starobinsky model, the corresponding initial conditions read  $V_0/m_P^4 = 10^{-10}$ ,  $\phi_i/m_P = 5.80$ , and  $\phi_{i,N}/m_P = -0.0137$ , and we have  $n_s = 0.9669$  and  $r = 0.00321$ , also consistent with the CMB constraints.

### 2.3 Power spectra and PBH abundance

To obtain the PBH abundance, we introduce the dimensionless power spectrum  $\mathcal{P}_{\mathcal{R}}(k)$  of  $\mathcal{R}_k$ ,

$$\mathcal{P}_{\mathcal{R}}(k) = \frac{k^3}{2\pi^2} |\mathcal{R}_k|^2 \Big|_{k \ll aH}. \quad (2.7)$$

Here, we should emphasize that, as  $\mathcal{R}_k$  can still evolve after exiting the Hubble horizon during the USR inflation,  $\mathcal{P}_{\mathcal{R}}(k)$  must be evaluated at the end of inflation, with the relevant scale satisfying  $k \ll aH$ .

Furthermore, we need to link  $\mathcal{P}_{\mathcal{R}}(k)$  to the dimensionless power spectrum  $\mathcal{P}_{\delta}(k)$  of the primordial density contrast  $\delta$ . In the radiation-dominated (RD) era, at the linear order, we have [207]

$$\mathcal{P}_{\delta}(k) = \frac{16}{81} \left( \frac{k}{aH} \right)^4 \mathcal{P}_{\mathcal{R}}(k).$$

By this relation, the  $i$ -th spectral moment  $\sigma_i$  of the density contrast  $\delta$  can be obtained as

$$\sigma_i^2(R) = \int_0^\infty \frac{dk}{k} k^{2i} \widetilde{W}^2(k, R) \mathcal{P}_{\delta}(k) = \frac{16}{81} \int_0^\infty \frac{dk}{k} k^{2i} \widetilde{W}^2(k, R) (kR)^4 \mathcal{P}_{\mathcal{R}}(k), \quad (2.8)$$

where  $i = 0, 1, 2, \dots$ , and  $\widetilde{W}(k, R)$  is the window function in the Fourier space, which smooths the perturbation over some physical scale  $R$ , often chosen as  $R = 1/(aH)$ . In this work, we choose Gaussian window function as  $\widetilde{W}^2(k, R) = e^{-k^2 R^2/2}$ , which prevents the issues related to the non-differentiability and divergence of the integral in the large- $k$  limit in Eq. (2.8).

For PBH formation, in the Carr–Hawking collapse model [91], the PBH mass  $M$  is related to the horizon mass  $M_{\text{H}}$  as

$$M = \kappa M_{\text{H}} = \kappa \frac{4\pi m_{\text{P}}^2}{H},$$

where  $\kappa$  is the collapse efficiency. Then, considering the conservation of entropy in the adiabatic cosmic expansion, we can obtain [104]

$$\frac{M}{M_{\odot}} = 1.13 \times 10^{15} \left( \frac{\kappa}{0.2} \right) \left( \frac{g_*}{106.75} \right)^{-1/6} \left( \frac{k_*}{k_{\text{PBH}}} \right)^2, \quad (2.9)$$

where  $M_{\odot} = 1.989 \times 10^{30}$  kg is the solar mass,  $g_*$  is the effective number of relativistic degrees of freedom of energy density,  $k_* = 0.05 \text{ Mpc}^{-1}$  is the CMB pivot scale for the Planck satellite experiment [158], and  $k_{\text{PBH}} = 1/R$  is the wave number of the PBH that exits the Hubble horizon. Below, we set  $\kappa = 0.2$  and  $g_* = 106.75$  in the RD era [92]. From Eq. (2.9), all spectral moments  $\sigma_i(R)$  can be reexpressed in terms of the PBH mass as  $\sigma_i(M)$ .

At the epoch of PBH formation in the RD era, its mass fraction  $\beta_{\text{PBH}}(M)$  is defined as

$$\beta_{\text{PBH}}(M) = \frac{\rho_{\text{PBH}}(M)}{\rho_{\text{R}}} \Big|_{\text{formation}},$$

where  $\rho_{\text{PBH}}(M)$  and  $\rho_{\text{R}}$  are the energy densities of PBH and radiation. Then, at the present time, the PBH abundance  $f_{\text{PBH}}(M)$  is defined as

$$f_{\text{PBH}}(M) = \frac{\rho_{\text{PBH}}(M)}{\rho_{\text{DM}}} \Big|_{\text{today}},$$

where  $\rho_{\text{DM}}$  is the energy density of DM. If we focus on monochromatic PBH mass,  $f_{\text{PBH}}(M)$  is naturally proportional to  $\beta_{\text{PBH}}(M)$  [104],

$$f_{\text{PBH}}(M) = 1.68 \times 10^8 \left( \frac{M}{M_{\odot}} \right)^{-1/2} \beta_{\text{PBH}}(M).$$

The PBH mass fraction  $\beta_{\text{PBH}}(M)$  can be calculated in different ways, corresponding to taking the spectral moments  $\sigma_i$  at different orders. In the general peak theory [208], all  $\sigma_0$ ,  $\sigma_1$ , and  $\sigma_2$  are needed, but the relevant calculations are rather tedious. A very convenient and effective simplification is the Green–Liddle–Malik–Sasaki approximation [207], which only consults  $\sigma_0$  and  $\sigma_1$  but yields almost the same results as peak theory. Hence, in this work, we will follow this approximation, which gives

$$\beta_{\text{PBH}}(M) = \frac{1}{\sqrt{2\pi}} Q^3 (\nu_c^2 - 1) e^{-\nu_c^2/2},$$

where  $Q = R\sigma_1/(\sqrt{3}\sigma_0)$ ,  $\nu_c = \delta_c/\sigma_0$  is the relative density contrast, and  $\delta_c$  is the threshold of  $\delta$  for PBH formation, which depends on many physical ingredients, such as the shape of the collapsing region [209–214], and the equation of state and the anisotropy of the cosmic medium [215–217]. In this work, we follow Ref. [211] and choose  $\delta_c = 0.414$ .

### 3 SIGWs

In this section, we provide a concise review of the derivation of the SIGW spectra in the RD era and at the present time.

#### 3.1 Basic equations

The equation of motion for the second-order tensor perturbation  $h_{ij}$  in Eq. (2.3) reads [21]

$$h''_{ij} + 2\mathcal{H}h'_{ij} - \nabla^2 h_{ij} = -4\mathcal{T}_{ij}^{lm}\mathcal{S}_{lm}, \quad (3.1)$$

where  $\mathcal{T}_{ij}^{lm}$  is the projection operator,  $\mathcal{S}_{lm}$  is the source term, a prime denotes the derivative with respect to the conformal time  $\tau$  defined as  $d\tau = dt/a(t)$ , and  $\mathcal{H} = a'/a$ . In the RD era, using the conformal Newtonian gauge, we have

$$\mathcal{S}_{ij} = 4\Psi\partial_i\partial_j\Psi + 2\partial_i\Psi\partial_j\Psi - \frac{1}{\mathcal{H}^2}\partial_i(\Psi' + \mathcal{H}\Psi)\partial_j(\Psi' + \mathcal{H}\Psi).$$

In general, the Fourier transform of  $h_{ij}$  is

$$h_{ij}(\tau, \mathbf{x}) = \int \frac{d^3k}{(2\pi)^{3/2}} e^{i\mathbf{k}\cdot\mathbf{x}} \left[ h_{\mathbf{k}}^+(\tau) e_{ij}^+(\mathbf{k}) + h_{\mathbf{k}}^\times(\tau) e_{ij}^\times(\mathbf{k}) \right],$$

where  $h_{\mathbf{k}}^+(\tau)$  and  $h_{\mathbf{k}}^\times(\tau)$  are the Fourier components of  $h_{ij}(\tau, \mathbf{x})$ , and  $e_{ij}^+(\mathbf{k})$  and  $e_{ij}^\times(\mathbf{k})$  are two time-independent polarization tensors that can be expressed in terms of two orthogonal basis vectors  $\mathbf{e}$  and  $\bar{\mathbf{e}}$  as

$$e_{ij}^+(\mathbf{k}) = \frac{1}{\sqrt{2}} [e_i(\mathbf{k})e_j(\mathbf{k}) - \bar{e}_i(\mathbf{k})\bar{e}_j(\mathbf{k})], \quad e_{ij}^\times(\mathbf{k}) = \frac{1}{\sqrt{2}} [e_i(\mathbf{k})\bar{e}_j(\mathbf{k}) + \bar{e}_i(\mathbf{k})e_j(\mathbf{k})].$$

In the Fourier space, Eq. (3.1) becomes

$$h_{\mathbf{k}}'' + 2\mathcal{H}h_{\mathbf{k}}' + k^2 h_{\mathbf{k}} = \mathcal{S}(\tau, \mathbf{k}), \quad (3.2)$$

where  $\mathcal{S}(\tau, \mathbf{k})$  is the Fourier transform of the source term  $\mathcal{S}_{lm}(\tau, \mathbf{x})$ , and we have ignored the polarization indices  $+$  and  $\times$ . Furthermore, we decompose the Fourier mode of the scalar perturbation  $\Psi$  as  $\Psi_{\mathbf{k}}(\tau) = \Psi(k\tau)\psi_{\mathbf{k}}$ , where  $\psi_{\mathbf{k}}$  is the initial value, and  $\Psi(k\tau)$  is the normalized transfer function. In the RD era, we have [24]

$$\Psi(k\tau) = \frac{9}{(k\tau)^2} \left[ \frac{\sin(k\tau/\sqrt{3})}{k\tau/\sqrt{3}} - \cos(k\tau/\sqrt{3}) \right].$$

In this way, the source term can be reexpressed as

$$\mathcal{S}(\tau, \mathbf{k}) = \int \frac{d^3k}{(2\pi)^{3/2}} e^{ij}(\mathbf{k}) \tilde{k}_i \tilde{k}_j f(\tau, \mathbf{k}, \tilde{\mathbf{k}}) \psi_{\mathbf{k}} \psi_{\mathbf{k}-\tilde{\mathbf{k}}},$$

where the source function  $f(\tau, \mathbf{k}, \tilde{\mathbf{k}})$  is [218]

$$\begin{aligned} f(\tau, \mathbf{k}, \tilde{\mathbf{k}}) &= 12\Psi(|\tilde{\mathbf{k}}|\tau)\Psi(|\mathbf{k}-\tilde{\mathbf{k}}|\tau) + 4\tau^2\Psi'(|\tilde{\mathbf{k}}|\tau)\Psi'(|\mathbf{k}-\tilde{\mathbf{k}}|\tau) \\ &\quad + 4\tau \left[ \Psi'(|\tilde{\mathbf{k}}|\tau)\Psi(|\mathbf{k}-\tilde{\mathbf{k}}|\tau) + \Psi(|\tilde{\mathbf{k}}|\tau)\Psi'(|\mathbf{k}-\tilde{\mathbf{k}}|\tau) \right]. \end{aligned}$$

With all above preparations, we can solve Eq. (3.2) by the Green function method,

$$h_{\mathbf{k}}(\tau) = \frac{1}{a(\tau)} \int d\tilde{\tau} G_k(\tau, \tilde{\tau}) a(\tilde{\tau}) \mathcal{S}(\tilde{\tau}, \mathbf{k}),$$

where the Green function is  $G_k(\tau, \tilde{\tau}) = \sin[k(\tau - \tilde{\tau})]/k$ .



### 3.2 SIGW spectra

The SIGW spectrum  $\Omega_{\text{GW}}$  is defined as the GW energy density  $\rho_{\text{GW}}$  per logarithmic wave number as

$$\Omega_{\text{GW}}(\tau, k) = \frac{1}{\rho_c} \frac{d\rho_{\text{GW}}(\tau, k)}{d \ln k},$$

where  $\rho_c$  is the critical energy density of the Universe. In the transverse-traceless gauge,  $\Omega_{\text{GW}}(\tau, k)$  can be written as [219, 220]

$$\Omega_{\text{GW}}(\tau, k) = \frac{1}{24} \left( \frac{k}{\mathcal{H}} \right)^2 \overline{\mathcal{P}_h(\tau, k)},$$

where  $\overline{(\cdots)}$  denotes the oscillation average, and  $\mathcal{P}_h(\tau, k)$  is the dimensionless power spectrum of the tensor perturbation  $h_{\mathbf{k}}$ , defined as

$$\mathcal{P}_h(\tau, k) = \frac{k^3}{2\pi^2} \delta_{\text{D}}(\mathbf{k} + \tilde{\mathbf{k}}) \langle h_{\mathbf{k}}(\tau) h_{\tilde{\mathbf{k}}}(\tau) \rangle,$$

where  $\delta_{\text{D}}$  is the Dirac  $\delta$  function, and the two-point correlation function  $\langle h_{\mathbf{k}}(\tau) h_{\tilde{\mathbf{k}}}(\tau) \rangle$  reads

$$\langle h_{\mathbf{k}}(\tau) h_{\tilde{\mathbf{k}}}(\tau) \rangle = \int \frac{d^3 q d^3 \tilde{q}}{(2\pi)^3} e^{ij}(\mathbf{k}) e^{lm}(\tilde{\mathbf{k}}) q_i q_j \tilde{q}_l \tilde{q}_m I(\tau, \mathbf{k}, \mathbf{q}) I(\tau, \tilde{\mathbf{k}}, \tilde{\mathbf{q}}) \langle \psi_{\mathbf{q}} \psi_{\mathbf{k}-\mathbf{q}} \psi_{\tilde{\mathbf{q}}} \psi_{\tilde{\mathbf{k}}-\tilde{\mathbf{q}}} \rangle, \quad (3.3)$$

with  $I(\tau, \mathbf{k}, \mathbf{q})$  being the kernel function,

$$I(\tau, \mathbf{k}, \mathbf{q}) = \int d\tilde{\tau} \frac{a(\tilde{\tau})}{a(\tau)} G_k(\tau, \tilde{\tau}) f(\tilde{\tau}, \mathbf{k}, \mathbf{q}).$$

Furthermore, by the Wick theorem, the four-point correlation function  $\langle \psi_{\mathbf{q}} \psi_{\mathbf{k}-\mathbf{q}} \psi_{\tilde{\mathbf{q}}} \psi_{\tilde{\mathbf{k}}-\tilde{\mathbf{q}}} \rangle$  in Eq. (3.3) can be decomposed as the sum of the products of two-point correlation functions. It is convenient to introduce three dimensionless variables as  $x = k\tau$ ,  $u = |\mathbf{k} - \tilde{\mathbf{k}}|/k$ , and  $v = |\tilde{\mathbf{k}}|/k$ . By this means,  $\mathcal{P}_h(\tau, k)$  can be obtained as

$$\mathcal{P}_h(\tau, k) = 4 \int_0^\infty dv \int_{|1-v|}^{1+v} du \left[ \frac{4v^2 - (1 + v^2 - u^2)^2}{4uv} \right]^2 \mathcal{I}^2(x, u, v) \mathcal{P}_{\mathcal{R}}(ku) \mathcal{P}_{\mathcal{R}}(kv),$$

where  $\mathcal{I}(x, u, v) = I(\tau, \mathbf{k}, \tilde{\mathbf{k}})k^2$  is the kernel function in terms of the dimensionless variables  $x$ ,  $u$ , and  $v$  [221]. In the RD era, the oscillation average of  $\mathcal{I}^2(x, u, v)$  in the late-time limit of  $x \rightarrow \infty$  is [24]

$$\begin{aligned} \overline{\mathcal{I}^2(x \rightarrow \infty, u, v)} &= \frac{1}{2} \left[ \frac{3(u^2 + v^2 - 3)^2}{4u^3 v^3 x} \right]^2 \left\{ \pi^2 (u^2 + v^2 - 3)^2 \Theta(u + v - \sqrt{3}) \right. \\ &\quad \left. + \left[ (u^2 + v^2 - 3) \ln \left| \frac{3 - (u+v)^2}{3 - (u-v)^2} \right| - 4uv \right]^2 \right\}, \end{aligned}$$

where  $\Theta$  is the Heaviside step function. We may further define two new variables as  $s = u + v$  and  $t = u - v$ . Taking into account  $\mathcal{H} = 1/\tau$  in the RD era, we obtain the SIGW spectrum

$\Omega_{\text{GW}}(\tau, k)$  as

$$\Omega_{\text{GW}}(\tau, k) = 12 \int_0^1 dt \int_1^\infty ds \frac{t(t^2 - 1)^2(s^2 - 1)^2(s^2 + t^2 - 6)^4}{(s^2 - t^2)^8} \\ \times \left\{ \left[ \ln \left| \frac{t^2 - 3}{s^2 - 3} \right| + \frac{2(s^2 - t^2)}{s^2 + t^2 - 6} \right]^2 + \pi^2 \Theta(s - \sqrt{3}) \right\} \mathcal{P}_{\mathcal{R}} \left( \frac{k}{2}(s + t) \right) \mathcal{P}_{\mathcal{R}} \left( \frac{k}{2}(s - t) \right).$$

Moreover, there is a simple relation between the wave number  $k$  and the frequency  $f$  of the SIGW [222],

$$f \approx 1.5 \times 10^{-15} \frac{k}{\text{Mpc}^{-1}} \text{ Hz}.$$

From this correspondence, we finally achieve the SIGW spectrum  $\Omega_{\text{GW}}(\tau, f)$  from  $\Omega_{\text{GW}}(\tau, k)$ .

Last, the SIGW spectrum at present time  $\Omega_{\text{GW}}(\tau_0, f)$  can be related to  $\Omega_{\text{GW}}(\tau_c, f)$  as

$$\Omega_{\text{GW}}(\tau_0, f) h^2 = \Omega_{\text{R}}^0 h^2 \frac{g_*(f)}{g_*^0} \left( \frac{g_{*s}^0}{g_{*s}(f)} \right)^{4/3} \Omega_{\text{GW}}(\tau_c, f),$$

where  $\Omega_{\text{R}}^0$  is the present energy density fraction of radiation,  $g_*$  and  $g_{*s}$  are the effective relativistic degrees of freedom that contribute to radiation energy and entropy densities, and  $\tau_c$  is some time after  $\Omega_{\text{GW}}(\tau, f)$  has become constant, as SIGWs can be regarded as a portion of radiation, so  $\Omega_{\text{GW}}(\tau_c, f)$  is an asymptotic constant during the RD era. In this work, we take the values  $\Omega_{\text{R}}^0 h^2 = 4.184 \times 10^{-5}$ ,  $g_*^0 = 3.383$ , and  $g_{*s}^0 = 3.930$ , respectively [223].

## 4 Bayesian analysis

In this section, we provide the elements of Bayesian analysis, including the likelihood function, prior and posterior distributions, and the Bayes factor between different models, respectively. The NANOGrav 15-year data set is also reviewed.

### 4.1 Likelihood function

The likelihood function  $\mathcal{L}$  is related to the timing residual  $\delta t$  of pulsars and can be expressed as [34, 36, 201]

$$\delta t = n + Fa + M\epsilon, \tag{4.1}$$

where  $\delta t$ ,  $n$ ,  $a$ , and  $\epsilon$  are column vectors, and  $F$  and  $M$  are matrices. Below, we explain Eq. (4.1) in more detail.

In Eq. (4.1),  $n$  is the white noise. The next term  $Fa$  describes the time-correlated stochastic process, including the intrinsic pulsar red noise and the GW signals. First,  $F$  is the Fourier basis matrix, composed of sines and cosines calculated from the time of arrival of the pulses with the frequency at  $f_i = i/T_{\text{obs}}$  ( $T_{\text{obs}} = 16.03$  yr is the time of arrival extent). Second,  $a$  is the amplitude, following a zero-mean normal distribution with the covariance matrix  $\langle aa^T \rangle = \phi$ , which is given by

$$[\phi]_{(ai)(bj)} = \delta_{ij}(\Gamma_{ab}\Phi_i + \delta_{ab}\varphi_{a,i}). \tag{4.2}$$

In Eq. (4.2), the subscripts  $a$  and  $b$  correspond to the pulsars,  $i$  and  $j$  represent the frequency harmonics,  $\Gamma_{ab}$  is the GW background overlap reduction function, denoting the mean correlation between pulsars  $a$  and  $b$  based on their angular separation in the sky, and the model-dependent coefficients  $\Phi_i$  can be related to the GW spectrum as

$$\Omega_{\text{GW}}(f)h^2 = \frac{h^2}{\rho_c^0} \frac{d\rho_{\text{GW}}(f)}{d \ln f} = \frac{8\pi^4 f^5}{H_0^2/h^2} \frac{\Phi(f)}{\Delta f},$$

where  $H_0 = 100h \text{ km s}^{-1} \text{ Mpc}^{-1}$  is the Hubble constant,  $\Phi(f)$  is defined as  $\Phi_i = \Phi(i/T_{\text{obs}})$ , and  $\Delta f = 1/T_{\text{obs}}$  is the width of the frequency bin. Moreover, in Eq. (4.2), the spectral component  $\varphi_{a,i} = \varphi_a(i/T_{\text{obs}})$  of the intrinsic pulsar noise is set in a power-law form as

$$\varphi_a(f) = \frac{A_a^2}{12\pi^2 T_{\text{obs}}} \left( \frac{f}{\text{yr}^{-1}} \right)^{-\gamma_a} \text{yr}^3,$$

where  $A_a$  is the intrinsic noise amplitude, and  $\gamma_a$  is the spectral index. Last, the term  $M\epsilon$  in Eq. (4.1) shows the uncertainty in the timing model, in which  $M$  is the design-matrix basis, and  $\epsilon$  is the coefficient.

We can marginalize over  $a$  and  $\epsilon$  to obtain the likelihood function  $\mathcal{L}$  that depends only on the parameters describing the red noise covariance matrix  $\langle aa^T \rangle$ ,

$$\mathcal{L}(\delta t | \phi) = \frac{1}{\sqrt{\det(2\pi C)}} \exp \left( -\frac{1}{2} \delta t^T C^{-1} \delta t \right),$$

where  $C = N + TBT^T$ , with  $N$  being the covariance matrix of  $n$ ,  $T = [M, F]$ , and  $B = \text{diag}(\infty, \phi)$ . Here,  $\infty$  is a diagonal matrix of infinities, implying that the priors for the parameters in  $\epsilon$  are assumed to be flat.

## 4.2 Data

The experimental data that we use in this work to constrain our model parameters in the inflaton potential come from two sides: PBHs and SIGWs. On the one side, the PBH abundance obtained from our model must obey the observational constraints in the relevant mass ranges. On the other side, for SIGWs, we consult the NANOGrav 15-year data set, containing the posterior distribution data of the time delay  $d(f)$  for 14 frequency bins and covering the frequency range from  $2.0 \times 10^{-9}$  to  $2.8 \times 10^{-8}$  Hz, which can be related to the power spectrum  $S(f)$  as  $S(f) = T_{\text{obs}} d(f)^2$ . Moreover, the energy density of the model-independent free GW spectrum  $\hat{\Omega}_{\text{GW}}(f)$  can be calculated from  $S(f)$  as

$$\hat{\Omega}_{\text{GW}}(f) = \frac{8\pi^4}{H_0^2} f^5 S(f).$$

Besides SIGWs, such a free GW spectrum can also be interpreted in other different ways. One possibility is the GW spectrum generated from SMBHBs [36],

$$\Omega_{\text{BHB}}(f) = \frac{2\pi^2}{3H_0^2} A_{\text{BHB}}^2 \left( \frac{f}{\text{yr}^{-1}} \right)^{5-\gamma_{\text{BHB}}} \text{yr}^{-2},$$

where  $A_{\text{BHB}}$  is the amplitude of intrinsic noise, with

$$\log_{10} A_{\text{BHB}} = -15.6_{-0.8}^{+0.7} \quad (68\% \text{ CL}),$$

and  $\gamma_{\text{BHB}}$  is the spectral index. Astrophysical and cosmological predictions suggest that the orbital evolution of binary star system driven solely by the GW emission follows

$$\gamma_{\text{BHB}} = \frac{13}{3}.$$

However, when  $\gamma_{\text{BHB}}$  is treated as a free parameter, its posterior distribution can be broader. Thus, in Sec. 5.3, both  $A_{\text{BHB}}$  and  $\gamma_{\text{BHB}}$  will also be considered as free model parameters in our Bayesian analysis.

### 4.3 Prior distributions and Bayes factor

In this work, unless otherwise specified, the prior distributions of the five model parameters  $\phi_0$ ,  $\sigma$ ,  $A_0$  (for the inflaton model),  $A_{\text{BHB}}$  and  $\gamma_{\text{BHB}}$  (for the SMBHBs) in the KKLT model are listed in Table 1 (those in the Starobinsky model are shown in App. A). The priors of  $\phi_0$ ,  $\sigma$ , and  $A_0$  are chosen as uniform distributions, and the priors of  $\log_{10} A_{\text{BHB}}$  and  $\gamma_{\text{BHB}}$  are the bivariate normal distribution, with the mean  $\boldsymbol{\mu}_{\text{BHB}}$  and covariance matrix  $\boldsymbol{\sigma}_{\text{BHB}}$  being

$$\boldsymbol{\mu}_{\text{BHB}} = \begin{pmatrix} -15.6 \\ 4.7 \end{pmatrix}, \quad \boldsymbol{\sigma}_{\text{BHB}} = \begin{pmatrix} 0.28 & -0.0026 \\ -0.0026 & 0.12 \end{pmatrix}.$$

Parameters	Priors
$\phi_0$	uniform in $[2.25, 2.50]$
$\sigma$	uniform in $[0.020, 0.027]$
$A_0$	uniform in $[-10^{-3}, 10^{-3}]$
$(\log_{10} A_{\text{BHB}}, \gamma_{\text{BHB}})$	normal( $\boldsymbol{\mu}_{\text{BHB}}, \boldsymbol{\sigma}_{\text{BHB}}$ )

**Table 1.** The prior distributions of the five model parameters  $\phi_0$ ,  $\sigma$ ,  $A_0$ ,  $A_{\text{BHB}}$ , and  $\gamma_{\text{BHB}}$ . The units of  $\phi_0$  and  $\sigma$  (i.e., the reduced Planck mass  $m_{\text{P}}$ ) are omitted for simplicity.

When comparing the preference of different models by the observational data, we usually calculate the Bayes factor  $\mathcal{B}_{12}$ , defined as [200]

$$\mathcal{B}_{12} = \frac{\mathcal{Z}_1}{\mathcal{Z}_2},$$

where the subscripts 1 and 2 correspond to two models, and  $\mathcal{Z}$  is the evidence of the relevant model,

$$\mathcal{Z} = \int \mathcal{L}(d|\theta) \pi(\theta) \text{d}\theta,$$

where  $d$  is the data,  $\theta$  is the model parameters,  $\mathcal{L}(d|\theta)$  is the likelihood function, and  $\pi(\theta)$  is the prior distribution, respectively.

## 5 Constraints on the inflaton potential in the KKLT model

By combining the SIGW spectrum  $\Omega_{\text{GW}}(f)$  obtained from our inflaton potential and the NANOGrav 15-year data set, we can constrain the model parameters. In this work, we

use the `PTArcade` code, which takes  $\Omega_{\text{GW}}(f)$  as input, samples the parameter space via the Markov Chain Monte Carlo method, and outputs the posterior distributions of the model parameters.

Our work consists of three steps in Secs. 5.1–5.3. In the first two steps, we regard the SIGWs as the unique source of the SGWB. Their difference is whether the plateau in the USR region is perfect or not, corresponding to two or three parameters in the inflaton potential. Moreover, the PBH abundance is taken into account in Sec. 5.2 to further reduce the allowed parameter space. Then, we also include the GWs from the SMBHBs and combine them with the SIGWs to understand the NANOGrav results. In this case, we will deal with five model parameters. Altogether, we wish to provide a thorough analysis of the NANOGrav 15-year data set with various possible interpretations.

Below, for clarity and conciseness, we focus on the KKL<sub>T</sub> model. All the analysis, figures, and discussions in the Starobinsky model are summarized in App. A, and we will find that the basic results and conclusions in these two models are very similar, supporting the generality of our work.

### 5.1 Case with two model parameters

To exhibit our calculation procedure and obtain preliminary insights for reference below, we start from the Bayesian analysis with only two model parameters: the position  $\phi_0$  and the width  $\sigma$  of the perturbation  $\delta V(\phi)$  on the background inflaton potential  $V_b(\phi)$ . This means that the third parameter  $A_0$  is fixed to be zero, in order to create a perfect plateau on  $V_b(\phi)$ . The prior distributions of  $\phi_0$  and  $\sigma$  are listed in Table 1, but for better illustration, we will use  $\log_{10} \sigma$  as the coordinate axes in all following figures, so  $\log_{10} \sigma \in [-1.699, -1.569]$ .

The posterior distributions of  $\phi_0$  and  $\sigma$  are displayed in Fig. 2. At the 68% CL, we have

$$\phi_0 = 2.382^{+0.027}_{-0.029}, \quad \log_{10} \sigma = -1.626^{+0.016}_{-0.014}. \quad (5.1)$$

Moreover, we clearly see a negative correlation between  $\phi_0$  and  $\sigma$ , with strong parameter degeneracy in their joint posterior distribution. This makes intuitive sense. With  $\sigma$  held constant, an increase of  $\phi_0$  not only shifts the peak position of the SIGW spectrum  $\Omega_{\text{GW}}(f)$ , but also increases its amplitude. Consequently,  $\sigma$  must be decreased to ensure that  $\Omega_{\text{GW}}(f)$  satisfies the observational constraints.

### 5.2 Case with three model parameters

Now, we extend our Bayesian analysis by taking the third model parameter  $A_0$  into account. This means that the plateau on  $V_b(\phi)$  is allowed to be inclined slightly. The prior distributions of  $\phi_0$ ,  $\sigma$ , and  $A_0$  can be found in Table 1, and we show our results in Fig. 3. At the 68% CL, we obtain the posterior distributions of  $\phi_0$  and  $\sigma$  as

$$\phi_0 = 2.387^{+0.025}_{-0.027}, \quad \log_{10} \sigma = -1.627^{+0.017}_{-0.014}. \quad (5.2)$$

These results remain basically the same as those in Eq. (5.1), but their joint posterior distribution has become broader compared with Fig. 2, indicating that the negative correlation between  $\phi_0$  and  $\sigma$  can be broken to some extent by the introduction of the third parameter  $A_0$ . Moreover, at the 68% CL, we obtain

$$A_0 = -2.197^{+4.054}_{-0.841} \times 10^{-4}. \quad (5.3)$$

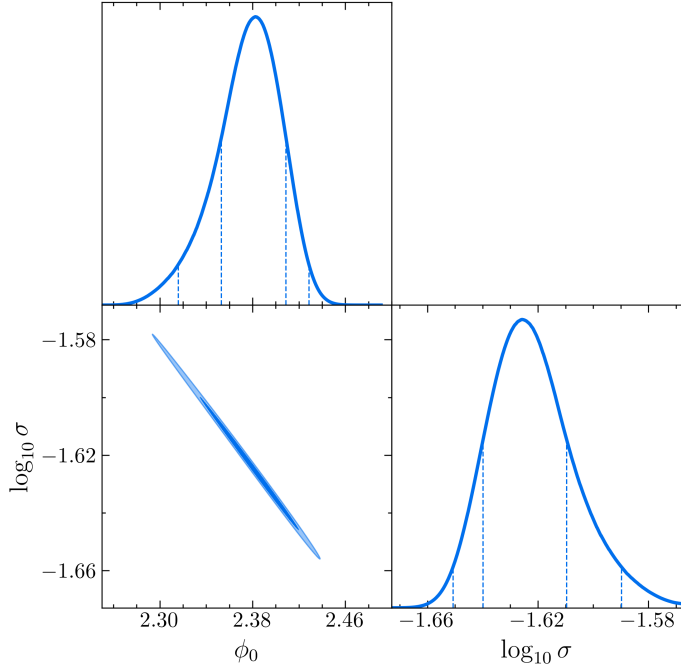


**Figure 2.** The posterior distributions of the two model parameters  $\phi_0$  and  $\sigma$  (both in the units of  $m_{\text{P}}$ ). The blue shaded areas correspond to the 68% and 95% CLs. At the 68% CL, we have  $\phi_0 = 2.382^{+0.027}_{-0.029}$  and  $\log_{10} \sigma = -1.626^{+0.016}_{-0.014}$ . It can be clearly seen that  $\phi_0$  and  $\sigma$  exhibit a negative correlation, with strong parameter degeneracy between them.

The posterior distribution of  $A_0$  peaks at a relatively small negative value of  $A_0 = -2.197 \times 10^{-4}$ , suggesting a positive slope of the plateau in the USR region. This result is physically reasonable and can be understood from two aspects. First, if the slope is too positive, the inflaton rolls down its potential too quickly, violating the USR condition. Second, if the slope is too negative, it is rather difficult for the inflaton to pass through the USR region. Therefore, we have adopted a narrow prior range for  $A_0$ , in order to avoid such situations.

Till now, we have merely considered the posterior distributions of the model parameters constrained by the NANOGrav 15-year data set. However, these parameters should not only guarantee the GW spectrum, but also must satisfy the constraints on the PBH abundance  $f_{\text{PBH}}$  at the same time. As a consequence, the parameter spaces in Fig. 3 are still too large. To address this, we calculate  $f_{\text{PBH}}$  with two different sets of model parameters, both satisfying the posterior distributions in Fig. 3. The first set is  $\phi_0 = 2.39$ ,  $\log_{10} \sigma = -1.631$ , and  $\log_{10} A_0 = -4.6$ , and the second set is  $\phi_0 = 2.41$ ,  $\log_{10} \sigma = -1.641$ , and  $\log_{10} A_0 = -4.5$ , with their comparison illustrated in Fig. 4. We find that the relevant PBH masses are both around  $10^{-3} M_{\odot}$ , where the observational constraints mainly come from the lensing experiments [224, 225]. It is obvious that the first set produces reasonable  $f_{\text{PBH}}$  (the solid black line), but the second set leads to strong contradiction with the experimental data (the dashed black line). Actually, we will discover that the majority of the parameter spaces in Fig. 3 results in an overproduction of PBHs, so they must be further constrained by  $f_{\text{PBH}}$ .<sup>1</sup>

<sup>1</sup>Here, we should mention that there would be a risk of PBH overproduction, if the SGWB around nHz frequencies seen by PTAs is attributed to the SIGWs from the Gaussian curvature perturbation [43]. To alle-

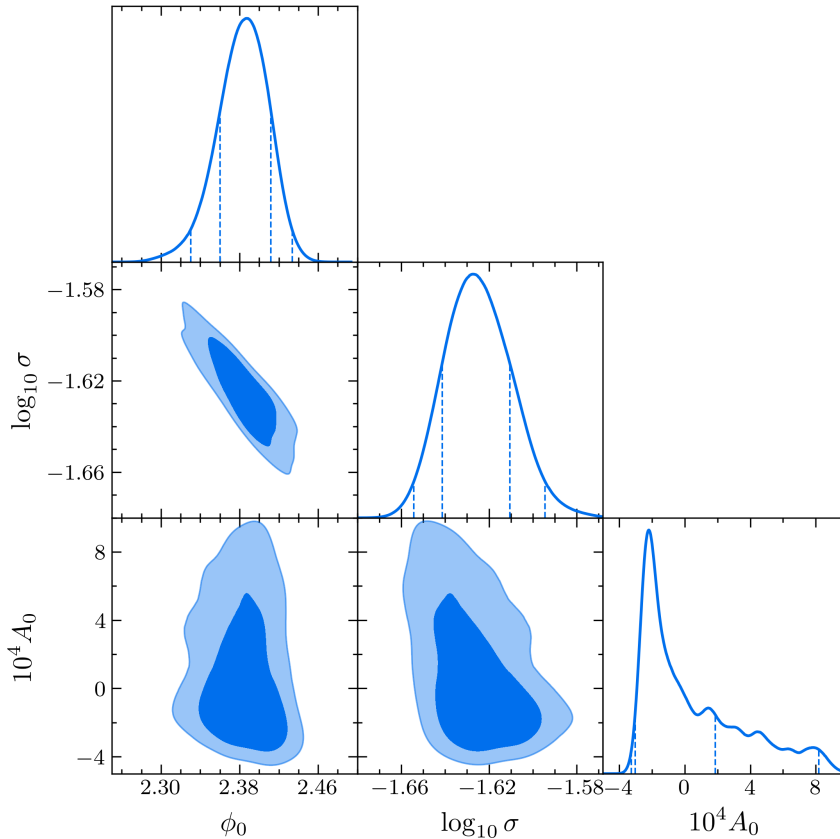


**Figure 3.** Same as Fig. 2, but with three model parameters  $\phi_0$ ,  $\sigma$ , and  $A_0$ . At the 68% CL, we obtain  $\phi_0 = 2.387^{+0.025}_{-0.027}$ ,  $\log_{10} \sigma = -1.627^{+0.017}_{-0.014}$ , and  $A_0 = -2.197^{+4.054}_{-0.841} \times 10^{-4}$ , respectively. The negative correlation between  $\phi_0$  and  $\sigma$  in their joint posterior distribution is somewhat broken by the introduction of  $A_0$ . In addition,  $A_0$  has high probability with relatively small negative values. This observation prefers the inflation model with a small positively sloped plateau in the USR region.

Consequently, it is essential to constrain the posterior distributions of the model parameters in order to satisfy the PBH abundance. To simplify this analysis, we take  $A_0$  as various constants:  $-2.197 \times 10^{-4}$  (the maximum marginal posterior value) and  $\pm 10^{-3}$  (the bounds of the prior distribution), and show the allowed regions in the joint posterior distribution of  $\phi_0$  and  $\sigma$  in Fig. 5. We find that the larger  $A_0$  is, the smaller the allowed region becomes. This observation indicates the decrease of  $\sigma$  with the increase of  $A_0$  (for the same  $\phi_0$ ), meaning that if the USR region has a negative slope, the plateau on the background potential must be narrow enough, so that the inflaton can roll down its potential definitely.

---

viate this problem, various attempts have been presented. The most common consideration is the introduction of non-Gaussianities [226, 227] (e.g., a negative non-Gaussianity [228–231] or a logarithmic non-Gaussianity [232]), but with some opposite opinions in Refs. [233, 234]. Other investigations can also be found in the literature, with the relevant topics on the domain wall networks [12], the scalar fluctuation propagation speed [119], the stiffer equation of state for the cosmic medium in the early Universe [132, 235], the axion–gauge dynamics [236], the power spectrum with finite-width [237], and the more complex inflation models (e.g., the curvaton scenario [238, 239], the inflation model with an additional spectator tensor field [240], the Galileon inflation model [241], the radiative hybrid inflation model [242], and the bounce model [243]).

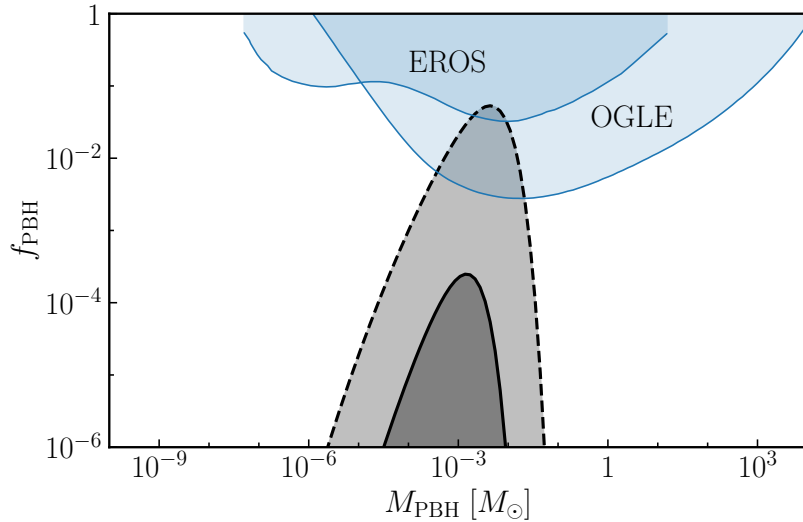


**Figure 4.** The PBH abundance  $f_{\text{PBH}}$  obtained with two different sets of model parameters. The solid black line with  $\phi_0 = 2.39$ ,  $\log_{10} \sigma = -1.631$ , and  $\log_{10} A_0 = -4.6$  gives reasonable  $f_{\text{PBH}}$ , but the dashed black line with  $\phi_0 = 2.41$ ,  $\log_{10} \sigma = -1.641$ , and  $\log_{10} A_0 = -4.5$  results in too large  $f_{\text{PBH}}$ , obviously in contradiction with the constraints from Expérience pour la Recherche d’Objets Sombres (EROS) [224] and Optical Gravitational Lensing Experiment (OGLE) [225]. This observation indicates that the majority of the parameter spaces in Fig. 3 leads to an overproduction of PBHs.

Below, we choose a specific set of model parameters:  $\phi_0 = 2.388$ ,  $\log_{10} \sigma = -1.623$ , and  $A_0 = -2.197 \times 10^{-4}$  as an example, which satisfy both the PBH and SIGW constraints, in order to discuss the scaling behaviors of the power spectrum  $\mathcal{P}_{\mathcal{R}}(k)$  and the SIGW spectrum  $\Omega_{\text{SIGW}}(f)$ . In Fig. 6, it can be clearly seen that  $\mathcal{P}_{\mathcal{R}}(k)$  exhibits the notable  $k^4$  scaling behavior in the steepest growth, consistent with both the numerical [244] and analytical results [245], then decreases approximately as  $k^{-0.10}$ , and finally drops on much smaller scales.<sup>2</sup> Moreover, the frequency dependence of  $\Omega_{\text{SIGW}}(f)$  is  $f^{2.65}$  in the infrared regime and  $f^{-0.20}$  in the ultraviolet regime. At even lower frequencies ( $\ll$  nHz), the  $f^3$  dependence of  $\Omega_{\text{SIGW}}(f)$  [25] is expected, but we do not show it here for simplicity.

Furthermore, by means of a modified version of the **SIGWfast** code [199], the envelope of the SIGW spectrum is plotted in Fig. 7, satisfying the PBH abundance constraint, with  $A_0 = -2.197 \times 10^{-4}$  and  $\phi_0$  and  $\sigma$  in the allowed region in their joint posterior distribution in Fig. 5. Thus, Fig. 6 can be regarded as a special case in Fig. 7. For comparison, we also include the sensitivity curves of three next-generation GW detectors: the Square Kilometer Array (SKA) [246], Laser Interferometer Space Antenna (LISA) [247], and Big Bang Observer (BBO) [248]. We observe that the SIGW spectrum obtained from our inflation model (the grey belt) not only successfully accounts for the NANOGrav 15-year data set with appropriate amplitude and spectral index, but is also detectable by the GW detectors in future. It should be mentioned that the currently observed signal in the PTA band may limit the sensitivities of the future detectors [249], but we will not consider it in this work.

<sup>2</sup>Generally speaking, the scaling behavior of  $\mathcal{P}_{\mathcal{R}}(k)$  on small scales depends on specific inflationary models. For more detailed discussions, see Refs. [196, 197].



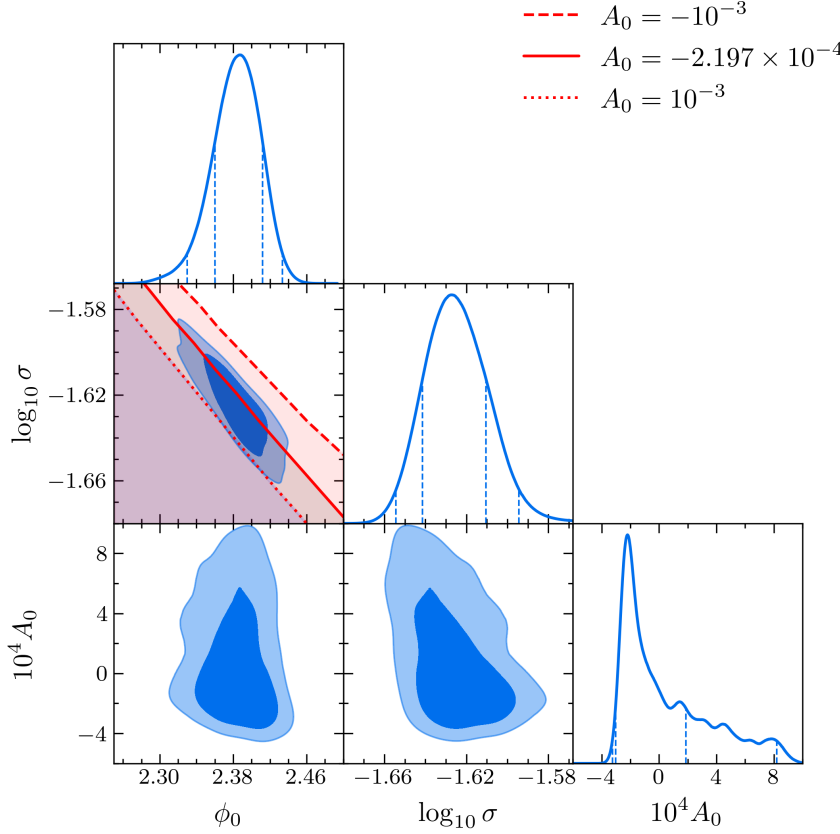


**Figure 5.** Same as Fig. 3, but with the constraints from the PBH abundance included. We take  $A_0$  as various constants and plot the allowed regions of  $\phi_0$  and  $\sigma$  in their joint posterior distribution. The overlapped regions with the contours represent the parameter spaces allowed for both the SIGW and PBH constraints (the solid red line for the maximum marginal posterior value  $A_0 = -2.197 \times 10^{-4}$ , and the dashed and dotted red lines for  $A_0 = -10^{-3}$  and  $10^{-3}$ , corresponding to its prior bounds). With the increase of  $A_0$ , the allowed region of  $\sigma$  decreases (for the same  $\phi_0$ ). This is because, when the slope at  $\phi_0$  becomes negative, the width of the USR region must be small, otherwise the inflaton cannot roll down its potential. The three lines with different  $A_0$  in the joint posterior distribution of  $\phi_0$  and  $\sigma$  are actually not straight. They seem so only because the prior ranges of  $\phi_0$  and  $\sigma$  are narrow.

### 5.3 Case with SMBHBs

Last, we consider the most general case with the impact of SMBHBs taken into account. SMBHBs can form during the hierarchical merging process of galaxies in structure formation, and their relevant SGWB lies in the PTA band [250–252]. Therefore, we will explore the scenario, in which the SGWB is composed of the SIGWs and the GWs emitted from SMBHBs together, so the total GW spectrum is

$$\Omega_{\text{GW}} = \Omega_{\text{SIGW}} + \Omega_{\text{BHB}}.$$

Now, we face the posterior distributions of five parameters:  $\phi_0$ ,  $\sigma$ ,  $A_0$  (for the inflation model),  $A_{\text{BHB}}$ , and  $\gamma_{\text{BHB}}$  (for the SMBHBs). Our results are presented in Figs. 8 and 9. At the 68%

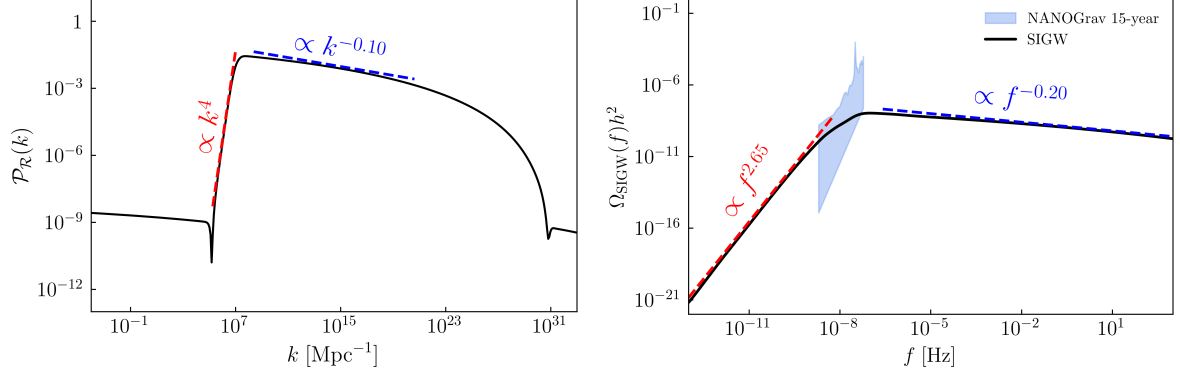


**Figure 6.** The scaling behaviors of the power spectrum  $\mathcal{P}_{\mathcal{R}}(k)$  (the left panel) and the SIGW spectrum  $\Omega_{\text{SIGW}}(f)$  (the right panel). The model parameters read  $\phi_0 = 2.388$ ,  $\log_{10} \sigma = -1.623$ , and  $A_0 = -2.197 \times 10^{-4}$ , so as to satisfy both the PBH and SIGW constraints.  $\mathcal{P}_{\mathcal{R}}(k)$  scales as  $k^4$  in the steepest growth, then decreases as  $k^{-0.10}$ , and finally drops on much smaller scales. Meanwhile,  $\Omega_{\text{SIGW}}(f)$  scales as  $f^{2.65}$  and  $f^{-0.20}$  in the infrared and ultraviolet regimes.

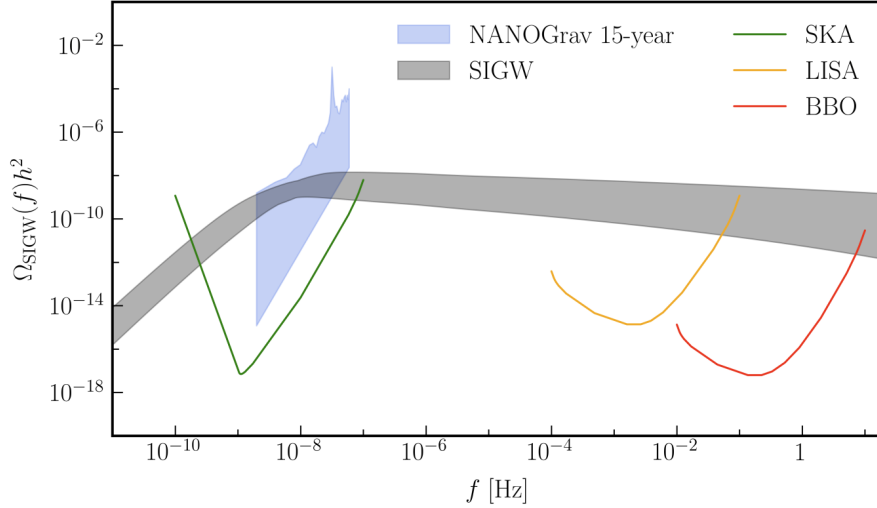


**Figure 7.** The envelope of the SIGW spectra  $\Omega_{\text{GW}}(f)$  (the grey belt) obtained from the model parameters satisfying both the constraints from the NANOGGrav 15-year data set and the PBH abundance, with  $A_0 = -2.197 \times 10^{-4}$ . The shaded light blue region represents the periodogram for the free spectral process from the NANOGGrav results, and our SIGW spectra pass through it with appropriate amplitudes and spectral indices. In addition, as the SIGW spectra are already above the sensitivity curves of three next-generation GW detectors: SKA, LISA, and BBO, the SIGWs are expected to be observed in future.

CL, we have

$$\phi_0 = 2.389^{+0.026}_{-0.030}, \quad (5.4)$$

$$\log_{10} \sigma = -1.629^{+0.020}_{-0.015}, \quad (5.5)$$

$$A_0 = -2.334^{+9.613}_{-0.882} \times 10^{-4}, \quad (5.6)$$

$$\log_{10} A_{\text{BHB}} = -15.646^{+0.467}_{-0.557}, \quad (5.7)$$

$$\gamma_{\text{BHB}} = 4.653^{+0.351}_{-0.414}. \quad (5.8)$$

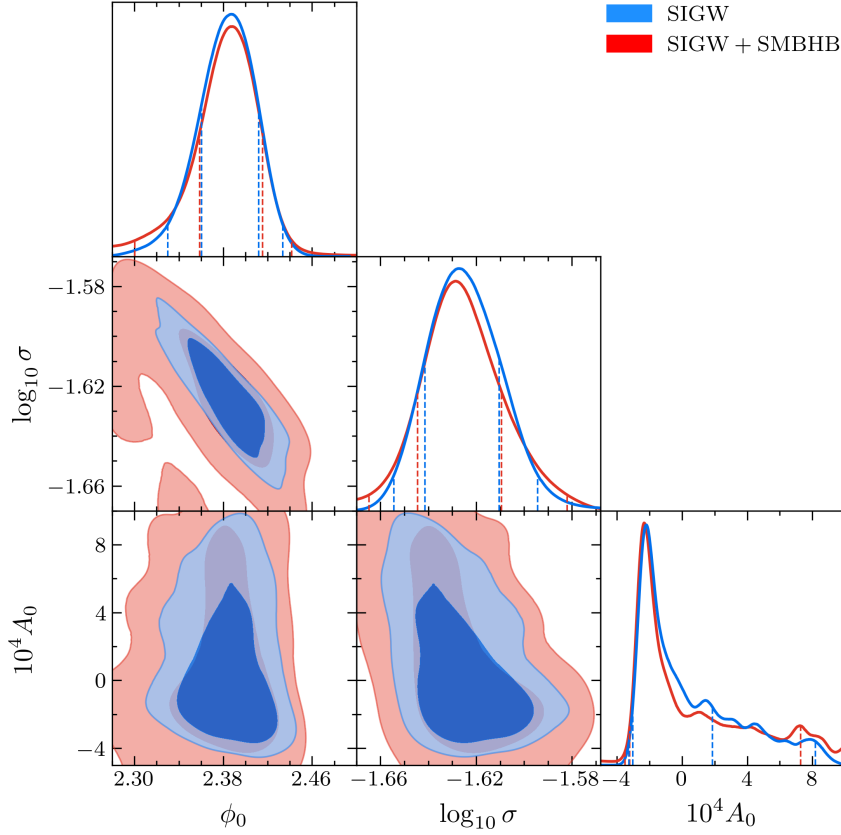


**Figure 8.** Same as Fig. 3, but with the impact of SMBHBs taken into account. The posterior distributions at the 68% CL read  $\phi_0 = 2.389^{+0.026}_{-0.030}$ ,  $\log_{10} \sigma = -1.629^{+0.020}_{-0.015}$ , and  $A_0 = -2.334^{+9.613}_{-0.882} \times 10^{-4}$ , respectively. We plot the three-parameter SIGW case and the five-parameter SIGW + SMBHB case together for comparison. The joint posterior distributions in the latter are broader. This is because, when only SIGW is considered, the GW spectrum from some parameter combinations is too low to account for the experimental data. However, if the contribution from SMBHBs is large enough, these combinations become allowed again.

From Eqs. (5.4)–(5.6) and Fig. 8, we observe that all the joint posterior distributions of  $\phi_0$ ,  $\sigma$ , and  $A_0$  become broader than those in the three-parameter case. This is because, when only SIGW is considered, the GW spectrum from some parameter combinations is too low to match the experimental data. However, as long as the contribution from SMBHBs is large enough, these parameter combinations again become allowed (e.g., within the 95% CL).

Furthermore, from Fig. 9, we notice that the posterior distribution of  $A_{\text{BHB}}$  has two peaks, reflecting the competition between SIGWs and SMBHBs. Different peak corresponds to different component that dominates the GW spectrum, consistent with the relevant analysis by the NANOGrav collaboration in Ref. [36]. When  $A_{\text{BHB}}$  is small, the GW spectrum is dominated by SIGWs; when  $A_{\text{BHB}}$  is large, the GW spectrum is driven by SMBHBs. Also, the spectral index  $\gamma_{\text{BHB}} = 13/3$  is within the 68% CL when it is treated as a free parameter.

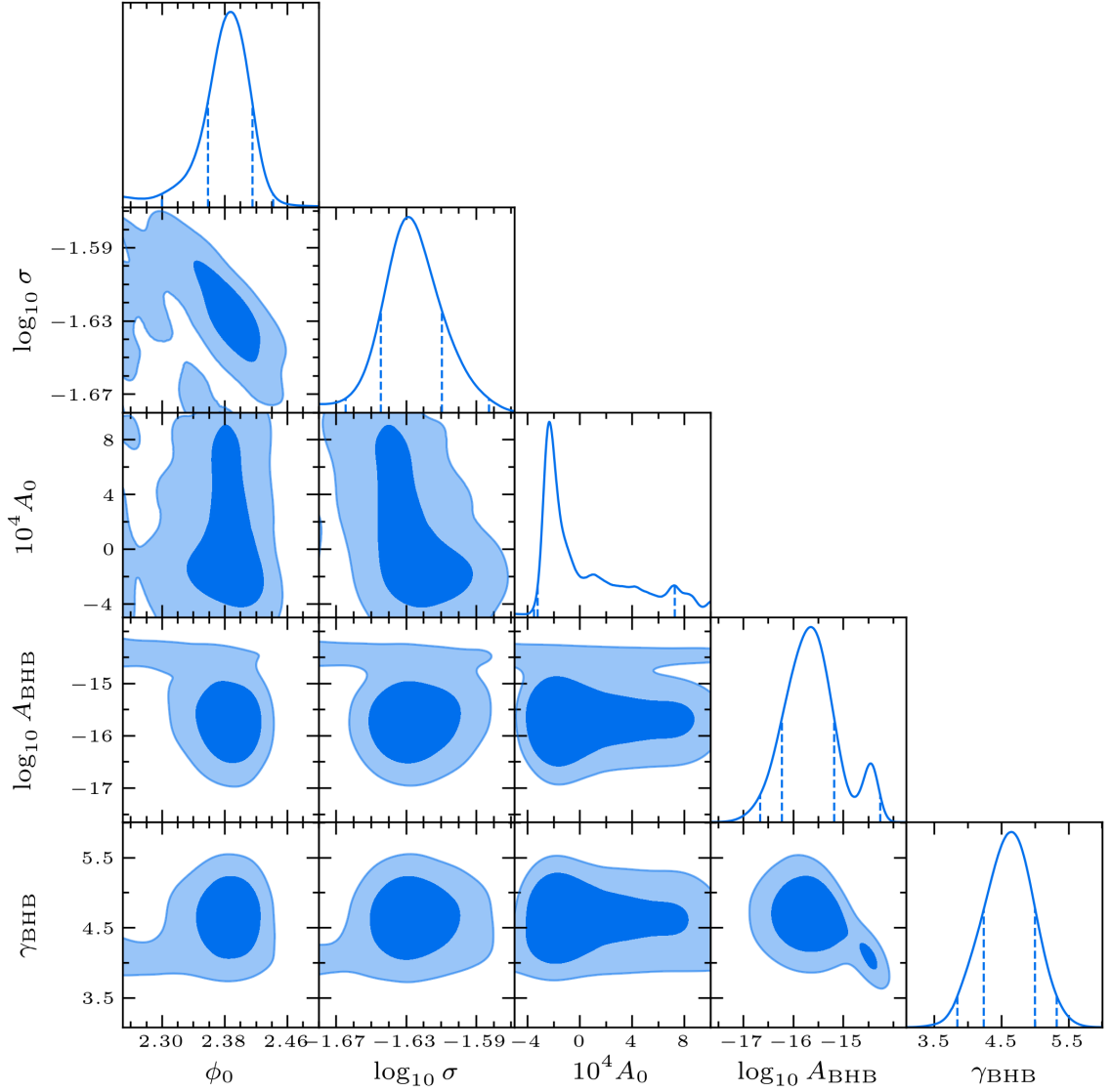


**Figure 9.** The posterior distributions of the model parameters with the impact of SMBHBs included. There are five model parameters altogether:  $\phi_0$ ,  $\sigma$ ,  $A_0$  (for the inflation model),  $A_{\text{BHB}}$ , and  $\gamma_{\text{BHB}}$  (for the SMBHBs). The posterior distribution of  $A_{\text{BHB}}$  has two peaks, reflecting the competition between SIGWs and SMBHBs. Different peak corresponds to different component that dominates the GW spectrum, consistent with the analysis by the NANOGrav collaboration in Ref. [36]. The value of the spectral index  $\gamma_{\text{BHB}} = 13/3$  is within its 68% CL when treated as a free parameter.

#### 5.4 Bayes factors

Finally, to complete our analysis, we calculate the Bayes factors between different models. With the parameters in Eqs. (5.1)–(5.8), the Bayes factor between the two-parameter and SMBHB-only models is

$$\mathcal{B} = \frac{\mathcal{Z}_{\text{SIGW}_2}}{\mathcal{Z}_{\text{SMBHB}}} = 20.21, \quad (5.9)$$

the Bayes factor between the three-parameter and SMBHB-only models is

$$\mathcal{B} = \frac{\mathcal{Z}_{\text{SIGW}_3}}{\mathcal{Z}_{\text{SMBHB}}} = 8.01, \quad (5.10)$$

and the Bayes factor between the five-parameter and SMBHB-only models is

$$\mathcal{B} = \frac{\mathcal{Z}_{\text{SIGW}_3 + \text{SMBHB}}}{\mathcal{Z}_{\text{SMBHB}}} = 7.36. \quad (5.11)$$

The above Bayes factors between different models reveal a clear hierarchy: the two-parameter model  $\text{SIGW}_2$  is strongly favored; the three-parameter model  $\text{SIGW}_3$  and the five-parameter model  $\text{SIGW}_3 + \text{SMBHB}$  are comparable but weaker. However, the fact that the two-parameter model has the largest Bayes factor may be merely caused by fixing  $A_0 = 0$  to realize a perfect plateau in the USR region. Since the SIGW spectrum essentially depend on three model parameters, we can only claim that the three-parameter model is slightly better than the five-parameter one, or equivalently, Bayesian analysis shows no preference with or without SMBHBs. This conclusion is comprehensible, because despite the increase of the number of free model parameters, the complex five-parameter model does not lead to a better fitting to the data. The likelihood does not change much, but meanwhile the prior space expands, so the five-parameter model is not superior to the three-parameter one. Nonetheless, all the two-, three-, and five-parameter models are significantly better than the SMBHB-only model, suggesting that the interpretation of the SGWB from the NANOGrav observations only via the GW spectrum from SMBHBs is not preferred in our inflation model.

## 6 Conclusion

The exploration on PBHs has aroused increasing interest in physics community in recent years. Besides its possibility as a natural candidate of DM and the source of BHB merger events, another research hotspot is the relevant SIGWs produced with PBHs simultaneously as a second-order effect. Since the detection of the potential SGWB in the PTA band, especially in the NANOGrav 15-year data set, SIGWs have become a promising interpretation in addition to the GWs from SMBHBs. To generate intensive SIGWs with certain amplitudes and frequencies, the usual SR inflation is not enough, and a USR phase is needed, in order to enhance the primordial power spectrum on small scales. The USR phase can be realized by imposing a perturbation on the background inflaton potential, and to determine the position and shape of this perturbation is the purpose of our work. For comparison, we verify the robustness of our conclusions against two different background inflaton potentials: the KKLt and Starobinsky models, and the similar results confirm the generality of our work.

In this paper, we construct an anti-symmetric perturbation  $\delta V(\phi)$  in Eq. (2.5) with three parameters:  $\phi_0$ ,  $\sigma$ , and  $A$  (or equivalently,  $A_0$  in Eq. (2.6)), describing the position, width, and slope of  $\delta V(\phi)$ , and these model parameters further determine the SIGW spectrum. In addition to the SIGWs from the USR inflation, we also consider the GW spectrum from SMBHBs, which is characterized by another two parameters: the amplitude  $A_{\text{BHB}}$  and spectral index  $\gamma_{\text{BHB}}$ . Altogether, we encounter the Bayesian analysis with five model parameters, which can be performed via the `PTArcade` code, with their prior distributions summarized in Tables 1 and 2.

Our work is composed of three steps. First, in order to reduce computation cost and obtain preliminary results for reference, we directly set the parameter  $A_0 = 0$ , so that the

plateau in the USR region is perfect. The posterior distributions of the two parameters  $\phi_0$  and  $\sigma$  can be found in Eq. (5.1), and we clearly observe the negative correlation in their joint posterior distribution in Fig. 2, with strong parameter degeneracy.

Then, we set  $A_0$  as a free parameter, meaning that the plateau in the USR region is allowed to be slightly inclined. In this three-parameter case, the joint posterior distribution of  $\phi_0$  and  $\sigma$  becomes broader, and the posterior distribution of  $A_0$  peaks at  $-2.197 \times 10^{-4}$ , as can be seen in Fig. 3. This feature indicates that a small positively sloped plateau on the background inflaton potential is preferred. Moreover, we find that some parameter spaces actually overproduce PBHs in certain mass region, as illustrated in Fig. 4. Thus, we further show the allowed parameter spaces in Fig. 5, which satisfy both the SIGW and PBH constraints. At last, we plot the SIGW spectrum in Fig. 7 and find that the SIGWs not only account for the SGWB, but are also detectable by the next-generation GW detectors.

Finally, we investigate the case with the impact of SMBHBs. We perform the full five-parameter Bayesian analysis, provide their posterior distributions in Figs. 8 and 9, and calculate the Bayes factors between different models in Eqs. (5.9)–(5.11). The Bayes factors indicate that the NANOGrav 15-year data set show preference for the two-parameter model, but this may be an artifact of fixing  $A_0 = 0$ . Hence, we can only confidently claim that all the two-, three-, and five-parameter models are significantly favored in Bayesian analysis than the SMBHB-only model.

Altogether, the overall circumstance seems not to be improved by increasing the number of free model parameters. Nevertheless, this tendency is consistent with Ref. [36], in which the NANOGrav collaboration analyzed the Bayes factors between different models with or without SMBHBs, concluding that some models perform better with considering SMBHBs, some are roughly equivalent, while others perform even worse. This primarily depends on whether the increase of model parameters provides a better fitting to the experimental data, and in our present work, it does not yield a substantially better fitting. Therefore, in summary, the simple two-parameter model with a perfect plateau in the USR region has the largest evidence, and is thus favored by the NANOGrav 15-year data set, though it may be just due to the demand that  $A_0$  vanishes. Moreover, the interpretation of the potential SGWB from the NANOGrav observations via only the GWs generated by SMBHBs is not preferred in our work, both in the KKLt and Starobinsky models.

Last, we should mention that we have not discussed the non-Gaussian effects in this work. This includes both the nonlinear relation between the primordial curvature perturbation  $\mathcal{R}$  and the density contrast  $\delta$ , as well as the intrinsic non-Gaussianity in  $\mathcal{R}$ . These non-Gaussianities may lead to notable shifts in the allowed parameter regions and different interpretations of the SGWB, and this will be the topic of our future studies.

## Acknowledgments

We thank Yi-Zhong Fan, Lei Feng, Gabriele Franciolini, Zhiping Jin, Xiao-Hui Liu, Dominik J. Schwarz, Bing-Yu Su, Ji-Xiang Zhao, and Xue Zhou for fruitful discussions. This work is supported by the Fundamental Research Funds for the Central Universities of China (No. N232410019).

## A Constraints on the inflaton potential in the Starobinsky model

In the Appendix, we show the Bayesian analysis of the three cases in the Starobinsky model. The contents below are parallel to those in Sec. 5. The priors of  $\phi_0$ ,  $\sigma$ , and  $A_0$  are chosen

as uniform distributions, and the priors of  $\log_{10} A_{\text{BHB}}$  and  $\gamma_{\text{BHB}}$  are the bivariate normal distribution, as listed in Table 2.

Parameters	Priors
$\phi_0$	uniform in $[4.8, 5.0]$
$\sigma$	uniform in $[0.017, 0.022]$
$A_0$	uniform in $[-10^{-3}, 10^{-3}]$
$(\log_{10} A_{\text{BHB}}, \gamma_{\text{BHB}})$	normal( $\boldsymbol{\mu}_{\text{BHB}}, \boldsymbol{\sigma}_{\text{BHB}}$ )

**Table 2.** The prior distributions of the five model parameters  $\phi_0$ ,  $\sigma$ ,  $A_0$ ,  $A_{\text{BHB}}$ , and  $\gamma_{\text{BHB}}$  in the Starobinsky model. The priors of  $A_0$ ,  $A_{\text{BHB}}$ , and  $\gamma_{\text{BHB}}$  are the same as those in the KKLT model, the prior of  $\sigma$  is also alike, but the prior of  $\phi_0$  shifts to larger values, as the inflaton sets out from larger initial position.

First, in the case with two model parameters, the posterior distributions of  $\phi_0$  and  $\sigma$  are plotted in Fig. 10. At the 68% CL, we have

$$\phi_0 = 4.929^{+0.024}_{-0.027}, \quad \log_{10} \sigma = -1.697^{+0.011}_{-0.010}.$$

Then, in the case with three model parameters, the posterior distributions of  $\phi_0$ ,  $\sigma$ , and  $A_0$  are shown in Fig. 11. At the 68% CL, we have

$$\phi_0 = 4.939^{+0.019}_{-0.024}, \quad \log_{10} \sigma = -1.697^{+0.009}_{-0.012}, \quad A_0 = -1.238^{+4.250}_{-1.313} \times 10^{-4}.$$

Last, in the case with SMBHBs, the posterior distributions of  $\phi_0$ ,  $\sigma$ ,  $A_0$ ,  $A_{\text{BHB}}$ , and  $\gamma_{\text{BHB}}$  are displayed in Fig. 12. At the 68% CL, we obtain

$$\begin{aligned} \phi_0 &= 4.938^{+0.023}_{-0.027}, \quad \log_{10} \sigma = -1.698^{+0.011}_{-0.013}, \quad A_0 = -1.280^{+4.573}_{-1.109} \times 10^{-4}, \\ \log_{10} A_{\text{BHB}} &= -15.654^{+0.465}_{-0.534}, \quad \gamma_{\text{BHB}} = 4.657^{+0.351}_{-0.375}. \end{aligned}$$

Finally, the Bayes factor between the two-parameter and SMBHB-only models is

$$\mathcal{B} = \frac{\mathcal{Z}_{\text{SIGW}_2}}{\mathcal{Z}_{\text{SMBHB}}} = 21.49, \quad (\text{A.1})$$

the Bayes factor between the three-parameter and SMBHB-only models is

$$\mathcal{B} = \frac{\mathcal{Z}_{\text{SIGW}_3}}{\mathcal{Z}_{\text{SMBHB}}} = 8.26, \quad (\text{A.2})$$

and the Bayes factor between the five-parameter and SMBHB-only models is

$$\mathcal{B} = \frac{\mathcal{Z}_{\text{SIGW}_3 + \text{SMBHB}}}{\mathcal{Z}_{\text{SMBHB}}} = 12.75. \quad (\text{A.3})$$

In summary, from various perspectives of the intuitive observation of the inflaton potentials, the posterior distributions of the model parameters, and the corresponding Bayes factors, the Starobinsky model exhibits significant similarity with the KKLT model. For instance, a slightly positive slope in the USR region is still preferred, and the SMBHB-only model is not favored by the data. The only difference between the two models is that their USR regions are at different positions, but this is understandable, as the potential in the Starobinsky model decreases more slowly than in the KKLT model.

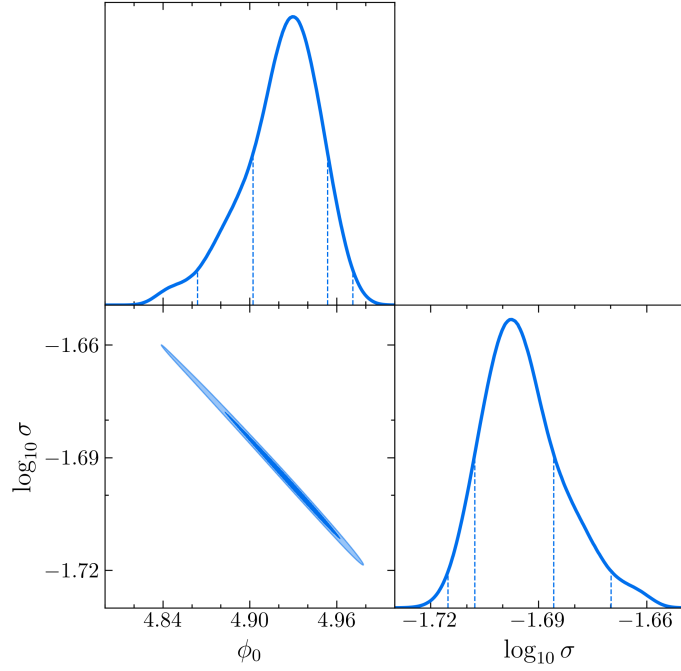


**Figure 10.** The posterior distributions of the model parameters  $\phi_0$  and  $\sigma$  in the Starobinsky model.

## References

- [1] B. P. Abbott *et al.* [LIGO Scientific and Virgo], *Observation of Gravitational Waves from a Binary Black Hole Merger*, Phys. Rev. Lett. **116**, 061102 (2016), [arXiv:1602.03837\[gr-qc\]](#).
- [2] R. Abbott *et al.* [KAGRA, VIRGO and LIGO Scientific], *GWTC-3: Compact Binary Coalescences Observed by LIGO and Virgo During the Second Part of the Third Observing Run*, Phys. Rev. X **13**, 041039 (2023), [arXiv:2111.03606\[gr-qc\]](#).
- [3] B. P. Abbott *et al.* [LIGO Scientific and Virgo], *GW170817: Observation of Gravitational Waves from a Binary Neutron Star Inspiral*, Phys. Rev. Lett. **119**, 161101 (2017), [arXiv:1710.05832\[gr-qc\]](#).
- [4] B. P. Abbott *et al.* [LIGO Scientific, Virgo, ..., and SKA South Africa/MeerKAT], *Multi-messenger Observations of a Binary Neutron Star Merger*, Astrophys. J. Lett. **848**, L12 (2017), [arXiv:1710.05833\[astro-ph.HE\]](#).
- [5] A. Kosowsky and M. S. Turner, *Gravitational Radiation from Colliding Vacuum Bubbles: Envelope Approximation to Many-Bubble Collisions*, Phys. Rev. D **47**, 4372 (1993), [arXiv:9211004\[astro-ph\]](#).
- [6] C. Grojean and G. Servant, *Gravitational Waves from Phase Transitions at the Electroweak Scale and Beyond*, Phys. Rev. D **75**, 043507 (2007), [arXiv:0607107\[hep-ph\]](#).
- [7] C. Caprini, M. Hindmarsh, S. Huber, T. Konstandin, J. Kozaczuk, G. Nardini, J. M. No, A. Petiteau, P. Schwaller, G. Servant, and D. J. Weir, *Science with the space-based interferometer eLISA. II: Gravitational waves from cosmological phase transitions*, J. Cosmol. Astropart. Phys. **04**, 001 (2016), [arXiv:1512.06239\[astro-ph.CO\]](#).
- [8] M. Hindmarsh, M. Lüben, J. Lumma, and M. Pauly, *Phase transitions in the early universe*, SciPost Phys. Lect. Notes **24**, 1 (2021), [arXiv:2008.09136\[astro-ph.CO\]](#).



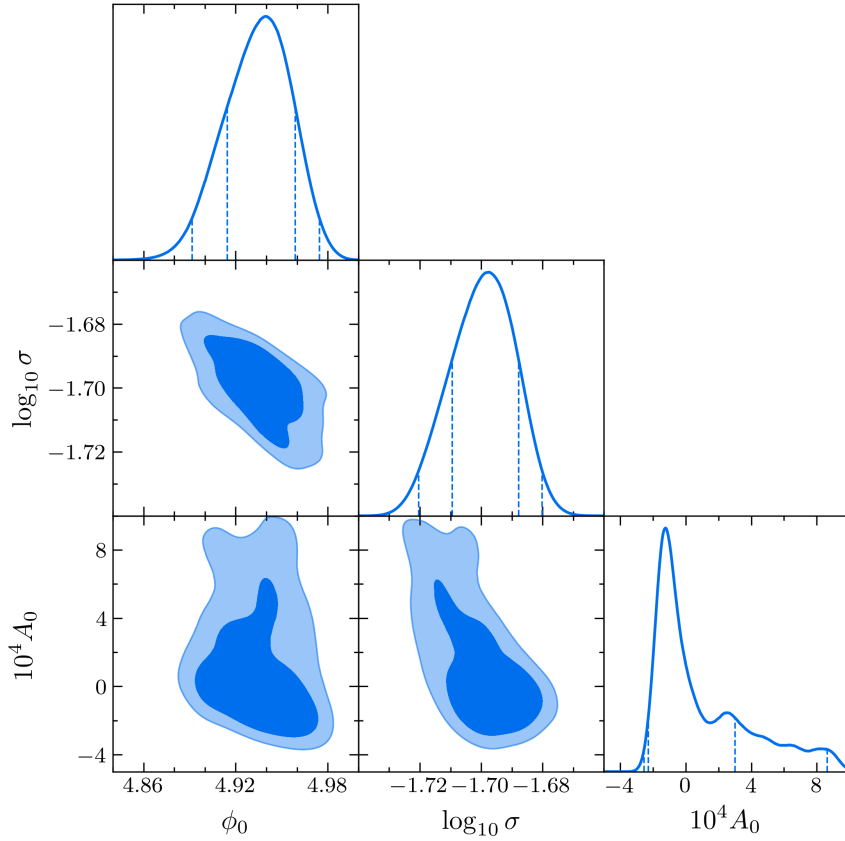


**Figure 11.** The posterior distributions of the model parameters  $\phi_0$ ,  $\sigma$ , and  $A_0$  in the Starobinsky model.

- [9] X. Martin and A. Vilenkin, *Gravitational wave background from hybrid topological defects*, Phys. Rev. Lett. **77**, 2879 (1996), [arXiv:9606022\[astro-ph\]](#).
- [10] D. G. Figueroa, M. Hindmarsh, and J. Urrestilla, *Exact Scale-Invariant Background of Gravitational Waves from Cosmic Defects*, Phys. Rev. Lett. **110**, 101302 (2013), [arXiv:1212.5458\[astro-ph.CO\]](#).
- [11] K. Saikawa, *A review of gravitational waves from cosmic domain walls*, Universe **3**, 40 (2017), [arXiv:1703.02576\[hep-ph\]](#).
- [12] Y. Gouttenoire and E. Vitagliano, *Domain wall interpretation of the PTA signal confronting black hole overproduction*, Phys. Rev. D **110**, L061306 (2024), [arXiv:2306.17841\[gr-qc\]](#).
- [13] D. G. Figueroa and F. Torrenti, *Gravitational wave production from preheating: parameter dependence*, J. Cosmol. Astropart. Phys. **10**, 057 (2017), [arXiv:1707.04533\[astro-ph.CO\]](#).
- [14] P. Adshead, J. T. Giblin, and Z. J. Weiner, *Gravitational waves from gauge preheating*, Phys. Rev. D **98**, 043525 (2018), [arXiv:1805.04550\[astro-ph.CO\]](#).
- [15] M. Giovannini, *Gravitational waves constraints on postinflationary phases stiffer than radiation*, Phys. Rev. D **58**, 083504 (1998), [arXiv:9806329\[hep-ph\]](#).
- [16] D. G. Figueroa and E. H. Tanin, *Ability of LIGO and LISA to probe the equation of state of the early Universe*, J. Cosmol. Astropart. Phys. **08**, 011 (2019), [arXiv:1905.11960\[astro-ph.CO\]](#).

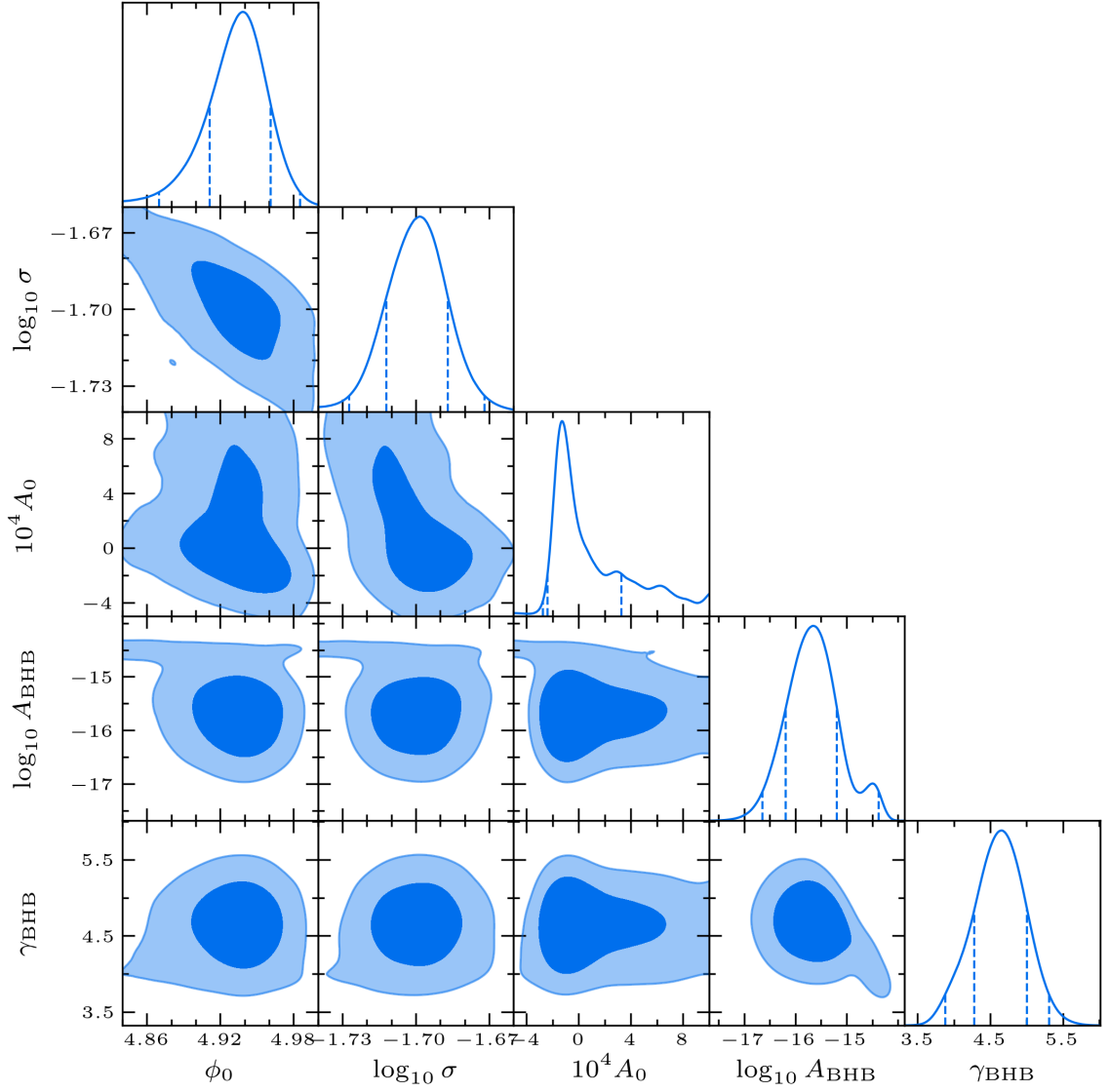


**Figure 12.** The posterior distributions of the model parameters  $\phi_0$ ,  $\sigma$ ,  $A_0$ ,  $A_{\text{BHB}}$ , and  $\gamma_{\text{BHB}}$  in the Starobinsky model.

- [17] R. T. Co, D. Dunskey, N. Fernandez, A. Ghalsasi, L. J. Hall, K. Harigaya, and J. Shelton, *Gravitational wave and CMB probes of axion kination*, J. High Energy Phys. **09**, 116 (2022), [arXiv:2108.09299\[hep-ph\]](#).
- [18] Y. Gouttenoire, G. Servant, and P. Simakachorn, *Kination cosmology from scalar fields and gravitational-wave signatures*, [arXiv:2111.01150\[hep-ph\]](#).
- [19] M. C. Guzzetti, N. Bartolo, M. Liguori, and S. Matarrese, *Gravitational waves from inflation*, Riv. Nuovo Cim. **39**, 399 (2016), [arXiv:1605.01615\[astro-ph.CO\]](#).
- [20] M. Peloso, L. Sorbo, and C. Unal, *Rolling axions during inflation: perturbativity and signatures*, J. Cosmol. Astropart. Phys. **09**, 001 (2016), [arXiv:1606.00459\[astro-ph.CO\]](#).

- [21] D. Baumann, P. Steinhardt, K. Takahashi, and K. Ichiki, *Gravitational Wave Spectrum Induced by Primordial Scalar Perturbations*, Phys. Rev. D **76**, 084019 (2007), [arXiv:0703290\[hep-th\]](#).
- [22] E. Bugaev and P. Klimai, *Induced gravitational wave background and primordial black holes*, Phys. Rev. D **81**, 023517 (2010), [arXiv:0908.0664\[astro-ph.CO\]](#).
- [23] J. R. Espinosa, D. Racco, and A. Riotto, *A Cosmological Signature of the SM Higgs Instability: Gravitational Waves*, J. Cosmol. Astropart. Phys. **09**, 012 (2018), [arXiv:1804.07732\[hep-ph\]](#).
- [24] K. Kohri and T. Terada, *Semianalytic Calculation of Gravitational Wave Spectrum Nonlinearly Induced from Primordial Curvature Perturbations*, Phys. Rev. D **97**, 123532 (2018), [arXiv:1804.08577\[gr-qc\]](#).
- [25] C. Yuan and Q.-G. Huang, *A topic review on probing primordial black hole dark matter with scalar induced gravitational waves*, iScience **24**, 102860 (2021), [arXiv:2103.04739\[astro-ph.GA\]](#).
- [26] M. Maggiore, *Gravitational wave experiments and early universe cosmology*, Phys. Rept. **331**, 283 (2000), [arXiv:9909001\[gr-qc\]](#).
- [27] C. Caprini and D. G. Figueroa, *Cosmological Backgrounds of Gravitational Waves*, Class. Quant. Grav. **35**, 163001 (2018), [arXiv:1801.04268\[astro-ph.CO\]](#).
- [28] J. Antoniadis *et al.* [EPTA and InPTA], *The second data release from the European Pulsar Timing Array III. Search for gravitational wave signals*, Astron. Astrophys. **678**, A50 (2023), [arXiv:2306.16214\[astro-ph.HE\]](#).
- [29] J. Antoniadis *et al.* [EPTA], *The second data release from the European Pulsar Timing Array I. The dataset and timing analysis*, Astron. Astrophys. **678**, A48 (2023), [arXiv:2306.16224\[astro-ph.HE\]](#).
- [30] D. J. Reardon *et al.*, *Search for an Isotropic Gravitational-wave Background with the Parkes Pulsar Timing Array*, Astrophys. J. Lett. **951**, L6 (2023), [arXiv:2306.16215\[astro-ph.HE\]](#).
- [31] A. Zic *et al.*, *The Parkes Pulsar Timing Array Third Data Release*, Publ. Astron. Soc. Austral. **40**, e049 (2023), [arXiv:2306.16230\[astro-ph.HE\]](#).
- [32] H. Xu *et al.*, *Searching for the nano-Hertz stochastic gravitational wave background with the Chinese Pulsar Timing Array Data Release I*, Res. Astron. Astrophys. **23**, 075024 (2023), [arXiv:2306.16216\[astro-ph.HE\]](#).
- [33] M. T. Miles *et al.*, *The MeerKAT Pulsar Timing Array: the first search for gravitational waves with the MeerKAT radio telescope*, Mon. Not. Roy. Astron. Soc. **536**, 1489 (2024), [arXiv:2412.01148\[astro-ph.HE\]](#).
- [34] G. Agazie *et al.* [NANOGrav], *The NANOGrav 15-year Data Set: Evidence for a Gravitational-Wave Background*, Astrophys. J. Lett. **951**, L8 (2023), [arXiv:2306.16213\[astro-ph.HE\]](#).
- [35] G. Agazie *et al.* [NANOGrav], *The NANOGrav 15 yr Data Set: Observations and Timing of 68 Millisecond Pulsars*, Astrophys. J. Lett. **951**, L9 (2023), [arXiv:2306.16217\[astro-ph.HE\]](#).
- [36] A. Afzal *et al.* [NANOGrav], *The NANOGrav 15-year Data Set: Search for Signals from New Physics*, Astrophys. J. Lett. **951**, L11 (2023), [arXiv:2306.16219\[astro-ph.HE\]](#).
- [37] G. Agazie *et al.* [NANOGrav], *The NANOGrav 15 yr Data Set: Constraints on Supermassive Black Hole Binaries from the Gravitational-wave Background*, Astrophys. J. Lett. **952**, L37 (2023), [arXiv:2306.16220\[astro-ph.HE\]](#).
- [38] R. W. Hellings and G. S. Downs, *Upper limits on the isotropic gravitational radiation background from pulsar timing analysis*, Astrophys. J. Lett. **265**, L39 (1983).
- [39] E. Madge, E. Morgante, C. Puchades-Ibáñez, N. Ramberg, W. Ratzinger, S. Schenk, and P. Schwaller, *Primordial gravitational waves in the nano-Hertz regime and PTA data—towards*

- solving the GW inverse problem*, J. High Energy Phys. **10**, 171 (2023), [arXiv:2306.14856\[hep-ph\]](#).
- [40] L. Zu, C. Zhang, Y.-Y. Li, Y. Gu, Y.-L. S. Tsai, and Y.-Z. Fan, *Mirror QCD phase transition as the origin of the nanohertz Stochastic Gravitational-Wave Background*, Sci. Bull. **69**, 741 (2024), [arXiv:2306.16769\[astro-ph.HE\]](#).
  - [41] S. Vagnozzi, *Inflationary interpretation of the stochastic gravitational wave background signal detected by pulsar timing array experiments*, J. High Energy Astrophys. **39**, 81 (2023), [arXiv:2306.16912\[astro-ph.CO\]](#).
  - [42] G. Franciolini, D. Racco, and F. Rompineve, *Footprints of the QCD Crossover on Cosmological Gravitational Waves at Pulsar Timing Arrays*, Phys. Rev. Lett. **132**, 081001 (2024), [arXiv:2306.17136\[astro-ph.CO\]](#).
  - [43] G. Franciolini, A. Iovino, Junior, V. Vaskonen, and H. Veermäe, *The Recent Gravitational Wave Observation by Pulsar Timing Arrays and Primordial Black Holes: The Importance of Non-Gaussianities*, Phys. Rev. Lett. **131**, 201401 (2023), [arXiv:2306.17149\[astro-ph.CO\]](#).
  - [44] Z. Wang, L. Lei, H. Jiao, L. Feng, and Y.-Z. Fan, *The nanohertz stochastic gravitational wave background from cosmic string loops and the abundant high redshift massive galaxies*, Sci. China Phys. Mech. Astron. **66**, 120403 (2023), [arXiv:2306.17150\[astro-ph.HE\]](#).
  - [45] A. Addazi, Y.-F. Cai, A. Marciano, and L. Visinelli, *Have pulsar timing array methods detected a cosmological phase transition?*, Phys. Rev. D **109**, 015028 (2024), [arXiv:2306.17205\[astro-ph.CO\]](#).
  - [46] P. Athron, A. Fowlie, C.-T. Lu, L. Morris, L. Wu, Y. Wu, and Z. Xu, *Can Supercooled Phase Transitions Explain the Gravitational Wave Background Observed by Pulsar Timing Arrays?*, Phys. Rev. Lett. **132**, 221001 (2024), [arXiv:2306.17239\[hep-ph\]](#).
  - [47] S. Jiang, A. Yang, J. Ma, and F.-P. Huang, *Implication of nano-Hertz stochastic gravitational wave on dynamical dark matter through a dark first-order phase transition*, Class. Quant. Grav. **41**, 065009 (2024), [arXiv:2306.17827\[hep-ph\]](#).
  - [48] P. F. Depta, K. Schmidt-Hoberg, P. Schwaller, and C. Tasillo, *Signals of merging supermassive black holes in pulsar timing arrays*, Phys. Rev. Res. **7**, 013196 (2025), [arXiv:2306.17836\[astro-ph.CO\]](#).
  - [49] D. Borah, S. Jyoti Das, and R. Samanta, *Imprint of inflationary gravitational waves and WIMP dark matter in pulsar timing array data*, J. Cosmol. Astropart. Phys. **03**, 031 (2024), [arXiv:2307.00537\[hep-ph\]](#).
  - [50] Y.-C. Bi, Y.-M. Wu, Z.-C. Chen, and Q.-G. Huang, *Implications for the supermassive black hole binaries from the NANOGrav 15-year data set*, Sci. China Phys. Mech. Astron. **66**, 120402 (2023), [arXiv:2307.00722\[astro-ph.CO\]](#).
  - [51] X. Niu and M. H. Rahat, *NANOGrav signal from axion inflation*, Phys. Rev. D **108**, 11 (2023), [arXiv:2307.01192\[hep-ph\]](#).
  - [52] I. Ben-Dayan, U. Kumar, U. Thattarampilly, and A. Verma, *Probing the early Universe cosmology with NANOGrav: Possibilities and limitations*, Phys. Rev. D **108**, 103507 (2023), [arXiv:2307.15123\[astro-ph.CO\]](#).
  - [53] K. T. Abe and Y. Tada, *Translating nano-Hertz gravitational wave background into primordial perturbations taking account of the cosmological QCD phase transition*, Phys. Rev. D **108**, L101304 (2023), [arXiv:2307.01653\[astro-ph.CO\]](#).
  - [54] T. Ghosh, A. Ghoshal, H.-K. Guo, F. Hajkarim, S. F. King, K. Sinha, X. Wang, and G. White, *Did we hear the sound of the Universe boiling? Analysis using the full fluid velocity profiles and NANOGrav 15-year data*, J. Cosmol. Astropart. Phys. **05**, 100 (2024), [arXiv:2307.02259\[astro-ph.HE\]](#).

- [55] L. Bian, S. Ge, J. Shu, B. Wang, X.-Y. Yang, and J. Zong, *Gravitational wave sources for pulsar timing arrays*, Phys. Rev. D **109**, L101301 (2024), [arXiv:2307.02376\[astro-ph.HE\]](#).
- [56] G. Servant and P. Simakachorn, *Constraining postinflationary axions with pulsar timing arrays*, Phys. Rev. D **108**, 12 (2023), [arXiv:2307.03121\[hep-ph\]](#).
- [57] Y.-M. Wu, Z.-C. Chen, and Q.-G. Huang, *Cosmological interpretation for the stochastic signal in pulsar timing arrays*, Sci. China Phys. Mech. Astron. **67**, 240412 (2024), [arXiv:2307.03141\[astro-ph.CO\]](#).
- [58] S. Choudhury, *Single field inflation in the light of Pulsar Timing Array Data: quintessential interpretation of blue tilted tensor spectrum through Non-Bunch Davies initial condition*, Eur. Phys. J. C **84**, 278 (2024), [arXiv:2307.03249\[astro-ph.CO\]](#).
- [59] Y. Gouttenoire, *First-Order Phase Transition Interpretation of Pulsar Timing Array Signal Is Consistent with Solar-Mass Black Holes*, Phys. Rev. Lett. **131**, 17 (2023), [arXiv:2307.04239\[hep-ph\]](#).
- [60] E. Babichev, D. Gorbunov, S. Ramazanov, R. Samanta, and A. Vikman, *NANOGrav spectral index  $\gamma = 3$  from melting domain walls*, Phys. Rev. D **108**, 123529 (2023), [arXiv:2307.04582\[hep-ph\]](#).
- [61] Z. Zhang, C. Cai, Y.-H. Su, S. Wang, Z.-H. Yu, and H.-H. Zhang, *Nano-Hertz gravitational waves from collapsing domain walls associated with freeze-in dark matter in light of pulsar timing array observations*, Phys. Rev. D **108**, 095037 (2023), [arXiv:2307.11495\[hep-ph\]](#).
- [62] B. Das, N. Jaman, and M. Sami, *Gravitational wave background from quintessential inflation and NANOGrav data*, Phys. Rev. D **108**, 103510 (2023), [arXiv:2307.12913\[gr-qc\]](#).
- [63] L. Liu, Z.-C. Chen, and Q.-G. Huang, *Probing the equation of state of the early Universe with pulsar timing arrays*, J. Cosmol. Astropart. Phys. **11**, 071 (2023), [arXiv:2307.14911\[astro-ph.CO\]](#).
- [64] J.-Q. Jiang, Y. Cai, G. Ye, and Y.-S. Piao, *Broken blue-tilted inflationary gravitational waves: a joint analysis of NANOGrav 15-year and BICEP/Keck 2018 data*, J. Cosmol. Astropart. Phys. **05**, 004 (2024), [arXiv:2307.15547\[astro-ph.CO\]](#).
- [65] H. An, B. Su, H. Tai, L.-T. Wang, and C. Yang, *Phase transition during inflation and the gravitational wave signal at pulsar timing arrays*, Phys. Rev. D **109**, L121304 (2024), [arXiv:2308.00070\[astro-ph.CO\]](#).
- [66] L. Frosina and A. Urbano, *Inflationary interpretation of the nHz gravitational-wave background*, Phys. Rev. D **108**, 103544 (2023), [arXiv:2308.06915\[astro-ph.CO\]](#).
- [67] S. He, L. Li, S. Wang, and S.-J. Wang, *Constraints on holographic QCD phase transitions from PTA observations*, Sci. China Phys. Mech. Astron. **68**, 210411 (2025), [arXiv:2308.07257\[hep-ph\]](#).
- [68] B. Cyr, T. Kite, J. Chluba, J. C. Hill, D. Jeong, S. K. Acharya, B. Bolliet, and S. P. Patil, *Disentangling the primordial nature of stochastic gravitational wave backgrounds with CMB spectral distortions*, Mon. Not. Roy. Astron. Soc. **528**, 883 (2024), [arXiv:2309.02366\[astro-ph.CO\]](#).
- [69] M. R. Gangopadhyay, V. V. Godithi, R. Inui, K. Ichiki, T. Kajino, A. Manusankar, G. J. Mathews, and Yogesh, *Is the NANOGrav detection evidence of resonant particle creation during inflation?*, J. High Energy Astrophys. **47**, 100358 (2025), [arXiv:2309.03101\[astro-ph.CO\]](#).
- [70] L. Liu, Y. Wu, and Z.-C. Chen, *Simultaneously probing the sound speed and equation of state of the early Universe with pulsar timing arrays*, J. Cosmol. Astropart. Phys. **04**, 011 (2024), [arXiv:2310.16500\[astro-ph.CO\]](#).
- [71] G. Sato-Polito, M. Zaldarriaga, and E. Quataert, *Where are the supermassive black holes measured by PTAs?*, Phys. Rev. D **110**, 063020 (2024), [arXiv:2312.06756\[astro-ph.CO\]](#).

- [72] S. Maity, N. Bhaumik, M. R. Haque, D. Maity, and L. Sriramkumar, *Constraining the history of reheating with the NANOGrav 15-year data*, J. Cosmol. Astropart. Phys. **01**, 118 (2025), [arXiv:2403.16963\[astro-ph.CO\]](#).
- [73] Z.-C. Chen and L. Liu, *Can we distinguish between adiabatic and isocurvature fluctuations with pulsar timing arrays?*, Sci. China Phys. Mech. Astron. **68**, 250412 (2025), [arXiv:2402.16781\[astro-ph.CO\]](#).
- [74] J. Kume and M. Hindmarsh, *Revised bounds on local cosmic strings from NANOGrav observations*, J. Cosmol. Astropart. Phys. **12**, 001 (2024), [arXiv:2404.02705\[astro-ph.CO\]](#).
- [75] M. R. Sah, S. Mukherjee, V. Saeedzadeh, A. Babul, M. Tremmel, and T. R. Quinn, *Imprints of supermassive black hole evolution on the spectral and spatial anisotropy of nano-hertz stochastic gravitational-wave background*, Mon. Not. Roy. Astron. Soc. **533**, 1568 (2024), [arXiv:2404.14508\[astro-ph.CO\]](#).
- [76] C. Smarra *et al.*, *Constraints on conformal ultralight dark matter couplings from the European Pulsar Timing Array*, Phys. Rev. D **110**, 043033 (2024), [arXiv:2405.01633\[astro-ph.HE\]](#).
- [77] P. Petrov, S. R. Taylor, M. Charisi, and C.-P. Ma, *Identifying the Host Galaxies of Supermassive Black Hole Binaries Found by Pulsar Timing Arrays*, Astrophys. J. **976**, 129 (2024), [arXiv:2406.04409\[astro-ph.GA\]](#).
- [78] B. Allen, D. Agarwal, J. D. Romano, and S. Valtolina, *Source anisotropies and pulsar timing arrays*, Phys. Rev. D **110**, 123507 (2024), [arXiv:2406.16031\[gr-qc\]](#).
- [79] P. F. Depta, V. Domcke, G. Franciolini, and M. Pieroni, *Pulsar timing array sensitivity to anisotropies in the gravitational wave background*, Phys. Rev. D **111**, 083039 (2025), [arXiv:2407.14460\[astro-ph.CO\]](#).
- [80] R. J. Truant, D. Izquierdo-Villalba, A. Sesana, G. M. Shaifullah, and M. Bonetti, *Resolving the nano-hertz gravitational wave sky: The detectability of eccentric binaries with PTA experiments*, Astron. Astrophys. **694**, A282 (2025), [arXiv:2407.12078\[astro-ph.GA\]](#).
- [81] E. R. Liepold and C.-P. Ma, *Big Galaxies and Big Black Holes: The Massive Ends of the Local Stellar and Black Hole Mass Functions and the Implications for Nanohertz Gravitational Waves*, Astrophys. J. Lett. **971**, L29 (2024), [arXiv:2407.14595\[astro-ph.GA\]](#).
- [82] T. Qiu and M. Zhu, *Interpreting pulsar timing array data of gravitational waves with Ekpyrosis-bouncing cosmology*, Phys. Rev. D **111**, 043508 (2025), [arXiv:2408.06582\[gr-qc\]](#).
- [83] T. Konstandin, A. M. Lemke, A. Mitridate, and E. Perboni, *The impact of cosmic variance on PTAs anisotropy searches*, J. Cosmol. Astropart. Phys. **04**, 059 (2025), [arXiv:2408.07741\[astro-ph.CO\]](#).
- [84] R. C. Bernardo and K.-W. Ng, *Charting the nanohertz gravitational wave sky with pulsar timing arrays*, Int. J. Mod. Phys. D **34**, 2540013 (2025), [arXiv:2409.07955\[astro-ph.CO\]](#).
- [85] Y. Chen, Q. Yu, and Y. Lu, *Constraining the Origin of the Nanohertz Gravitational-wave Background by Pulsar Timing Array Observations of Both the Background and Individual Supermassive Binary Black Holes*, Astrophys. J. **974**, 261 (2024), [arXiv:2409.18029\[astro-ph.HE\]](#).
- [86] P. Athron, M. Chianese, S. Datta, R. Samanta, and N. Saviano, *Impact of memory-burdened black holes on primordial gravitational waves in light of Pulsar Timing Array*, J. Cosmol. Astropart. Phys. **05**, 005 (2025), [arXiv:2411.19286\[astro-ph.CO\]](#).
- [87] P. Conzini, G. Fanizza, M. Gasperini, E. Pavone, L. Tedesco, and G. Veneziano, *Constraints on the Pre-Big Bang scenario from a cosmological interpretation of the NANOGrav data*, J. Cosmol. Astropart. Phys. **02**, 039 (2025), [arXiv:2412.01734\[hep-ph\]](#).



- [88] J. Ellis, M. Fairbairn, G. Franciolini, G. Hütsi, A. Iovino, M. Lewicki, M. Raidal, J. Urrutia, V. Vaskonen, and H. Veermäe, *What is the source of the PTA GW signal?*, Phys. Rev. D **109**, 023522 (2024), [arXiv:2308.08546\[astro-ph.CO\]](#).
- [89] D. G. Figueroa, M. Pieroni, A. Ricciardone, and P. Simakachorn, *Cosmological Background Interpretation of Pulsar Timing Array Data*, Phys. Rev. Lett. **132**, 171002 (2024), [arXiv:2307.02399\[astro-ph.CO\]](#).
- [90] S. W. Hawking, *Gravitationally collapsed objects of very low mass*, Mon. Not. Roy. Astron. Soc. **152**, 75 (1971).
- [91] B. J. Carr and S. W. Hawking, *Black Holes in the Early Universe*, Mon. Not. Roy. Astron. Soc. **168**, 399 (1974).
- [92] B. J. Carr, *The primordial black hole mass spectrum*, Astrophys. J. **201**, 1 (1975).
- [93] M. Yu. Khlopov, *Primordial Black Holes*, Res. Astron. Astrophys. **10**, 495 (2010), [arXiv:0801.0116\[astro-ph.CO\]](#).
- [94] S. Bird, I. Cholis, J. B. Muñoz, Y. Ali-Haïmoud, M. Kamionkowski, E. D. Kovetz, A. Raccanelli, and A. G. Riess, *Did LIGO detect dark matter?*, Phys. Rev. Lett. **116**, 201301 (2016), [arXiv:1603.00464\[astro-ph.CO\]](#).
- [95] S. Clesse and J. García-Bellido, *The clustering of massive Primordial Black Holes as Dark Matter: measuring their mass distribution with Advanced LIGO*, Phys. Dark Univ. **15**, 142 (2017), [arXiv:1603.05234\[astro-ph.CO\]](#).
- [96] M. Sasaki, T. Suyama, T. Tanaka, and S. Yokoyama, *Primordial Black Hole Scenario for the Gravitational-Wave Event GW150914*, Phys. Rev. Lett. **117**, 061101 (2016), [arXiv:1603.08338\[astro-ph.CO\]](#).
- [97] S. Clesse and J. García-Bellido, *Massive Primordial Black Holes from Hybrid Inflation as Dark Matter and the seeds of Galaxies*, Phys. Rev. D **92**, 023524 (2015), [arXiv:1501.07565\[astro-ph.CO\]](#).
- [98] J. L. Bernal, A. Raccanelli, L. Verde, and J. Silk, *Signatures of primordial black holes as seeds of supermassive black holes*, J. Cosmol. Astropart. Phys. **05**, 017 (2018), [arXiv:1712.01311\[astro-ph.CO\]](#).
- [99] B. Carr and J. Silk, *Primordial Black Holes as Generators of Cosmic Structures*, Mon. Not. Roy. Astron. Soc. **478**, 3756 (2018), [arXiv:1801.00672\[astro-ph.CO\]](#).
- [100] G.-W. Yuan, L. Lei, Y.-Z. Wang, B. Wang, Y.-Y. Wang, C. Chen, Z.-Q. Shen, Y.-F. Cai, and Y.-Z. Fan, *Rapidly growing primordial black holes as seeds of the massive high-redshift JWST Galaxies*, Sci. China Phys. Mech. Astron. **67**, 109512 (2024), [arXiv:2303.09391\[astro-ph.CO\]](#).
- [101] B.-Y. Su, N. Li, and L. Feng, *An inflation model for massive primordial black holes to interpret the JWST observations*, [arXiv:2306.05364\[astro-ph.CO\]](#).
- [102] B. Carr, F. Kühnel, and M. Sandstad, *Primordial Black Holes as Dark Matter*, Phys. Rev. D **94**, 083504 (2016), [arXiv:1607.06077\[astro-ph.CO\]](#).
- [103] B. Carr, S. Clesse, J. García-Bellido, and F. Kühnel, *Cosmic conundra explained by thermal history and primordial black holes*, Phys. Dark Univ. **31**, 100755 (2021), [arXiv:1906.08217\[astro-ph.CO\]](#).
- [104] B. Carr, K. Kohri, Y. Sendouda, and J. Yokoyama, *Constraints on Primordial Black Holes*, Rept. Prog. Phys. **84**, 116902 (2021), [arXiv:2002.12778\[astro-ph.CO\]](#).
- [105] B. Carr and F. Kühnel, *Primordial Black Holes as Dark Matter: Recent Developments*, Ann. Rev. Nucl. Part. Sci. **70**, 355 (2020), [arXiv:2006.02838\[astro-ph.CO\]](#).

- [106] A. M. Green and B. J. Kavanagh, *Primordial Black Holes as a dark matter candidate*, J. Phys. G **48**, 043001 (2021), [arXiv:2007.10722\[astro-ph.CO\]](#).
- [107] A. Escrivà, F. Kühnel, and Y. Tada, *Primordial Black Holes*, [arXiv:2211.05767\[astro-ph.CO\]](#).
- [108] J.-P. Li, S. Wang, Z.-C. Zhao, and K. Kohri, *Primordial non-Gaussianity  $f_{\text{NL}}$  and anisotropies in scalar-induced gravitational waves*, J. Cosmol. Astropart. Phys. **10**, 056 (2023), [arXiv:2305.19950\[astro-ph.CO\]](#).
- [109] H.-L. Huang, Y. Cai, J.-Q. Jiang, J. Zhang, and Y.-S. Piao, *Supermassive Primordial Black Holes for Nano-Hertz Gravitational Waves and High-redshift JWST Galaxies*, Res. Astron. Astrophys. **24**, 091001 (2024), [arXiv:2306.17577\[gr-qc\]](#).
- [110] Y.-F. Cai, X.-C. He, X.-H. Ma, S.-F. Yan, and G.-W. Yuan, *Limits on scalar-induced gravitational waves from the stochastic background by pulsar timing array observations*, Sci. Bull. **68**, 2929 (2023), [arXiv:2306.17822\[gr-qc\]](#).
- [111] K. Inomata, K. Kohri, and T. Terada, *Detected stochastic gravitational waves and subsolar-mass primordial black holes*, Phys. Rev. D **109**, 063506 (2024), [arXiv:2306.17834\[astro-ph.CO\]](#).
- [112] Y. Gouttenoire, S. Trifinopoulos, G. Valogiannis, and M. Vanvlasselaer, *Scrutinizing the primordial black hole interpretation of PTA gravitational waves and JWST early galaxies*, Phys. Rev. D **109**, 123002 (2024), [arXiv:2307.01457\[astro-ph.CO\]](#).
- [113] C. Unal, A. Papageorgiou, and I. Obata, *Axion-gauge dynamics during inflation as the origin of pulsar timing array signals and primordial black holes*, Phys. Lett. B **856**, 138873 (2024), [arXiv:2307.02322\[astro-ph.CO\]](#).
- [114] Z. Yi, Q. Gao, Y. Gong, Y. Wang, and F. Zhang, *Scalar induced gravitational waves in light of Pulsar Timing Array data*, Sci. China Phys. Mech. Astron. **66**, 120404 (2023), [arXiv:2307.02467\[gr-qc\]](#).
- [115] S. Wang, Z.-C. Zhao, and Q.-H. Zhu, *Constraints on scalar-induced gravitational waves up to third order from a joint analysis of BBN, CMB, and PTA data*, Phys. Rev. Res. **6**, 013207 (2024), [arXiv:2307.03095\[astro-ph.CO\]](#).
- [116] Z.-Q. You, Z. Yi, and Y. Wu, *Constraints on primordial curvature power spectrum with pulsar timing arrays*, J. Cosmol. Astropart. Phys. **11**, 065 (2023), [arXiv:2307.04419\[gr-qc\]](#).
- [117] S. A. Hosseini Mansoori, F. Felegray, A. Talebian, and M. Sami, *PBHs and GWs from  $T^2$ -inflation and NANOGrav 15-year data*, J. Cosmol. Astropart. Phys. **08**, 067 (2023), [arXiv:2307.06757\[astro-ph.CO\]](#).
- [118] K. Cheung, C. J. Ouseph, and P.-Y. Tseng, *NANOGrav and other PTA signals and PBH from the modified Higgs inflation*, Eur. Phys. J. C **84**, 906 (2024), [arXiv:2307.08046\[hep-ph\]](#).
- [119] S. Balaji, G. Domènech, and G. Franciolini, *Scalar-induced gravitational wave interpretation of PTA data: the role of scalar fluctuation propagation speed*, J. Cosmol. Astropart. Phys. **10**, 041 (2023), [arXiv:2307.08552\[gr-qc\]](#).
- [120] Z. Yi, Z.-Q. You, and Y. Wu, *Model-independent reconstruction of the primordial curvature power spectrum from PTA data*, J. Cosmol. Astropart. Phys. **01**, 066 (2024), [arXiv:2308.05632\[astro-ph.CO\]](#).
- [121] N. Bhaumik, R. K. Jain, and M. Lewicki, *Ultralow mass primordial black holes in the early Universe can explain the pulsar timing array signal*, Phys. Rev. D **108**, 123532 (2023), [arXiv:2308.07912\[astro-ph.CO\]](#).
- [122] Z. Yi, Z.-Q. You, Y. Wu, Z.-C. Chen, and L. Liu, *Exploring the NANOGrav signal and planet-mass primordial black holes through Higgs inflation*, J. Cosmol. Astropart. Phys. **06**, 043 (2024), [arXiv:2308.14688\[astro-ph.CO\]](#).



- [123] K. Harigaya, K. Inomata, and T. Terada, *Induced gravitational waves with kination era for recent pulsar timing array signals*, Phys. Rev. D **108**, 123538 (2023), [arXiv:2309.00228\[astro-ph.CO\]](#).
- [124] J.-P. Li, S. Wang, Z.-C. Zhao, and K. Kohri, *Complete analysis of the background and anisotropies of scalar-induced gravitational waves: primordial non-Gaussianity  $f_{NL}$  and  $g_{NL}$  considered*, J. Cosmol. Astropart. Phys. **06**, 039 (2024), [arXiv:2309.07792\[astro-ph.CO\]](#).
- [125] M. Tagliazucchi, M. Braglia, F. Finelli, and M. Pieroni, *Quest for CMB spectral distortions to probe the scalar-induced gravitational wave background interpretation of pulsar timing array data*, Phys. Rev. D **111**, 2 (2025), [arXiv:2310.08527\[astro-ph.CO\]](#).
- [126] S. Heydari, and K. Karami, *Primordial black holes and secondary gravitational waves from generalized power-law non-canonical inflation with quartic potential*, Eur. Phys. J. C **84**, 127 (2024), [arXiv:2310.11030\[gr-qc\]](#).
- [127] A. Nassiri-Rad and K. Asadi, *Induced Gravitational Waves from Non-attractor Inflation and NANOGrav data*, J. Cosmol. Astropart. Phys. **04**, 009 (2024), [arXiv:2310.11427\[astro-ph.CO\]](#).
- [128] Z. Chang, Y.-T. Kuang, D. Wu, and J.-Z. Zhou, *Probing scalar induced gravitational waves with PTA and LISA: the importance of third order correction*, J. Cosmol. Astropart. Phys. **04**, 044 (2024), [arXiv:2312.14409\[astro-ph.CO\]](#).
- [129] Z.-C. Chen, J. Li, L. Liu, and Z. Yi, *Probing the speed of scalar-induced gravitational waves with pulsar timing arrays*, Phys. Rev. D **109**, L101302 (2024), [arXiv:2401.09818\[gr-qc\]](#).
- [130] R. Z. Ferreira, A. Notari, O. Pujolàs, and F. Rompineve, *Collapsing domain wall networks: impact on pulsar timing arrays and primordial black holes*, J. Cosmol. Astropart. Phys. **06**, 020 (2024), [arXiv:2401.14331\[astro-ph.CO\]](#).
- [131] A. Iannicari, A. J. Iovino, A. Kehagias, D. Perrone, and A. Riotto, *Primordial black hole abundance: The importance of broadness*, Phys. Rev. D **109**, 123549 (2024), [arXiv:2402.11033\[astro-ph.CO\]](#).
- [132] G. Domènech, S. Pi, A. Wang, and J. Wang, *Induced Gravitational Wave interpretation of PTA data: a complete study for general equation of state*, J. Cosmol. Astropart. Phys. **08**, 054 (2024), [arXiv:2402.18965\[astro-ph.CO\]](#).
- [133] G. Perna, C. Testini, A. Ricciardone, and S. Matarrese, *Fully non-Gaussian Scalar-Induced Gravitational Waves*, J. Cosmol. Astropart. Phys. **05**, 086 (2024), [arXiv:2403.06962\[astro-ph.CO\]](#).
- [134] T. Papanikolaou, S. Banerjee, Y.-F. Cai, S. Capozziello, and E. N. Saridakis, *Primordial black holes and induced gravitational waves in non-singular matter bouncing cosmology*, J. Cosmol. Astropart. Phys. **06**, 066 (2024), [arXiv:2404.03779\[gr-qc\]](#).
- [135] A. Escrivà, R. Inui, Y. Tada, and C. M. Yoo, *LISA forecast on a smooth crossover beyond the standard model through the scalar-induced gravitational waves*, Phys. Rev. D **111**, 023528 (2025), [arXiv:2404.12591\[astro-ph.CO\]](#).
- [136] G. Domènech and A. Ganz, *Enhanced induced gravitational waves in Horndeski gravity*, J. Cosmol. Astropart. Phys. **01**, 020 (2025), [arXiv:2406.19950\[gr-qc\]](#).
- [137] A. J. Iovino, G. Perna, A. Riotto, and H. Veermäe, *Curbing PBHs with PTAs*, J. Cosmol. Astropart. Phys. **10**, 050 (2024), [arXiv:2406.20089\[astro-ph.CO\]](#).
- [138] A. Afzal, A. Ghoshal, and S. F. King, *Primordial Black Holes and Scalar-induced Gravitational Waves in Sneutrino Hybrid Inflation*, Phys. Rev. D **111**, 023050 (2025), [arXiv:2407.15082\[astro-ph.CO\]](#).

- [139] J.-Z. Zhou, Y.-T. Kuang, D. Wu, H. Lü, and Z. Chang, *Induced gravitational waves for arbitrary higher orders: Vertex rules and loop diagrams in cosmological perturbation theory*, Phys. Rev. D **111**, 083512 (2025), [arXiv:2408.14052\[astro-ph.CO\]](#).
- [140] S. Datta and R. Samanta, *Cosmic superstrings, metastable strings and ultralight primordial black holes: from NANOGrav to LIGO and beyond*, J. High Energy Phys. **02**, 095 (2025), [arXiv:2409.03498\[gr-qc\]](#).
- [141] K. Kohri, T. Terada, and T. T. Yanagida, *Induced gravitational waves probing primordial black hole dark matter with the memory burden effect*, Phys. Rev. D **111**, 063543 (2025), [arXiv:2409.06365\[astro-ph.CO\]](#).
- [142] J.-Z. Zhou, Y.-T. Kuang, D. Wu, F.-Y. Chen, H. Lü, and Z. Chang, *Scalar induced gravitational waves in  $f(R)$  gravity*, J. Cosmol. Astropart. Phys. **12**, 021 (2024), [arXiv:2409.07702\[gr-qc\]](#).
- [143] G. Domènech and J. Tränkle, *From formation to evaporation: Induced gravitational wave probes of the primordial black hole reheating scenario*, Phys. Rev. D **111**, 063528 (2025), [arXiv:2409.12125\[gr-qc\]](#).
- [144] R. Maji, A. Moursy, and Q. Shafi, *Induced gravitational waves, metastable cosmic strings and primordial black holes in GUTs*, J. Cosmol. Astropart. Phys. **01**, 106 (2025), [arXiv:2409.13584\[hep-ph\]](#).
- [145] S. Choudhury, *Reconstructing inflationary potential from NANOGrav 15-year data: A robust study using Non-Bunch Davies initial condition*, J. High Energy Astrophys. **44**, 220 (2024), [arXiv:2410.11893\[gr-qc\]](#).
- [146] J.-Z. Zhou, Y.-T. Kuang, Z. Chang, and H. Lü, *Constraints on Primordial Black Holes from  $N_{eff}$ : Scalar-induced Gravitational Waves as an Extra Radiation Component*, Astrophys. J. **979**, 178 (2025), [arXiv:2410.10111\[astro-ph.CO\]](#).
- [147] R. Picard and M. W. Davies, *Effects of scalar non-Gaussianity on induced scalar-tensor gravitational waves*, J. Cosmol. Astropart. Phys. **02**, 037 (2025), [arXiv:2410.17819\[astro-ph.CO\]](#).
- [148] A. J. Iovino, S. Matarrese, G. Perna, A. Ricciardone, and A. Riotto, *How Well Do We Know the Scalar-Induced Gravitational Waves?*, [arXiv:2412.06764\[astro-ph.CO\]](#).
- [149] S. Allegrini, L. Del Grosso, A. J. Iovino, and A. Urbano, *Is the formation of primordial black holes from single-field inflation compatible with standard cosmology?*, [arXiv:2412.14049\[astro-ph.CO\]](#).
- [150] D. Wu, J.-Z. Zhou, Y.-T. Kuang, Z.-C. Li, Z. Chang, and Q.-G. Huang, *Can tensor-scalar induced GWs dominate PTA observations?*, J. Cosmol. Astropart. Phys. **03**, 045 (2025), [arXiv:2501.00228\[astro-ph.CO\]](#).
- [151] P.-B. Chen and T.-J. Gao, *Gravitational waves and primordial black holes from the T-model inflation with Gauss-Bonnet correction*, [arXiv:2501.12242\[astro-ph.CO\]](#).
- [152] L.-S. Wang, L.-Y. Chen, and Q.-T. Xie, *Primordial black holes and scalar induced gravitational waves from sound speed resonance in derivatively coupling inflation model*, [arXiv:2503.01460\[astro-ph.CO\]](#).
- [153] D. Nandi, R. Roy, S. Yadav, and A. Sarkar, *Sub-Horizon Amplification of Curvature Perturbations: A New Route to Primordial Black Holes and Gravitational Waves*, [arXiv:2504.16059\[astro-ph.CO\]](#).
- [154] L. Barack *et al.*, *Black holes, gravitational waves and fundamental physics: a roadmap*, Class. Quant. Grav. **36**, 143001 (2019), [arXiv:1806.05195\[gr-qc\]](#).

- [155] H. V. Ragavendra and L. Sriramkumar, *Observational Imprints of Enhanced Scalar Power on Small Scales in Ultra Slow Roll Inflation and Associated Non-Gaussianities*, *Galaxies* **11**, 34 (2023), [arXiv:2301.08887\[astro-ph.CO\]](#).
- [156] B. Carr, S. Clesse, J. García-Bellido, M. Hawkins, and F. Kühnel, *Observational evidence for primordial black holes: A positivist perspective*, *Phys. Rept.* **1054**, 1 (2024), [arXiv:2306.03903\[astro-ph.CO\]](#).
- [157] E. Bagui *et al.* [LISA Cosmology Working Group], *Primordial black holes and their gravitational-wave signatures*, *Living Rev. Rel.* **28**, 1 (2025), [arXiv:2310.19857\[astro-ph.CO\]](#).
- [158] Y. Akrami *et al.* [Planck], *Planck 2018 results. X. Constraints on inflation*, *Astron. Astrophys.* **641**, A10 (2020), [arXiv:1807.06211\[astro-ph.CO\]](#).
- [159] C. Germani and T. Prokopec, *On primordial black holes from an inflection point*, *Phys. Dark Univ.* **18**, 6 (2017), [arXiv:1706.04226\[astro-ph.CO\]](#).
- [160] K. Dimopoulos, *Ultra slow-roll inflation demystified*, *Phys. Lett. B* **775**, 262 (2017), [arXiv:1707.05644\[hep-ph\]](#).
- [161] H. Di and Y. Gong, *Primordial black holes and second order gravitational waves from ultra-slow-roll inflation*, *J. Cosmol. Astropart. Phys.* **07**, 007 (2018), [arXiv:1707.09578\[astro-ph.CO\]](#).
- [162] A. Ashoorioon, A. Rostami, and J. T. Firouzjaee, *Examining the end of inflation with primordial black holes mass distribution and gravitational waves*, *Phys. Rev. D* **103**, 123512 (2021), [arXiv:2012.02817\[astro-ph.CO\]](#).
- [163] S. Pi, Y.-l. Zhang, Q.-G. Huang, and M. Sasaki, *Scalaron from  $R^2$ -gravity as a Heavy Field*, *J. Cosmol. Astropart. Phys.* **05**, 042 (2018), [arXiv:1712.09896\[astro-ph.CO\]](#).
- [164] J. Lin, Q. Gao, Y. Gong, Y. Lu, C. Zhang, and F. Zhang, *Primordial black holes and secondary gravitational waves from  $k$  and  $G$  inflation*, *Phys. Rev. D* **101**, 103515 (2020), [arXiv:2001.05909\[gr-qc\]](#).
- [165] S. Saburov and S. V. Ketov, *Quantum loop corrections in the modified gravity model of Starobinsky inflation with primordial black hole production*, *Universe* **10**, 354 (2024), [arXiv:2402.02934\[gr-qc\]](#).
- [166] L. Wu, Y. Gong, and T. Li, *Primordial black holes and secondary gravitational waves from string inspired general no-scale supergravity*, *Phys. Rev. D* **104**, 123544 (2021), [arXiv:2105.07694\[gr-qc\]](#).
- [167] R. Ishikawa and S. V. Ketov, *Exploring the parameter space of modified supergravity for double inflation and primordial black hole formation*, *Class. Quant. Grav.* **39**, 015016 (2022), [arXiv:2108.04408\[astro-ph.CO\]](#).
- [168] R. Ishikawa and S. V. Ketov, *Improved model of large-field inflation with primordial black hole production in Starobinsky-like supergravity*, *Class. Quant. Grav.* **41**, 195014 (2024), [arXiv:2401.11651\[astro-ph.CO\]](#).
- [169] J. M. Ezquiaga, J. García-Bellido, and E. R. Morales, *Primordial Black Hole production in Critical Higgs Inflation*, *Phys. Lett. B* **776**, 345 (2018), [arXiv:1705.04861\[astro-ph.CO\]](#).
- [170] M. Cicoli, V. A. Diaz, and F. G. Pedro, *Primordial Black Holes from String Inflation*, *J. Cosmol. Astropart. Phys.* **06**, 034 (2018), [arXiv:1803.02837\[hep-th\]](#).
- [171] I. Dalianis, A. Kehagias, and G. Tringas, *Primordial Black Holes from  $\alpha$ -attractors*, *J. Cosmol. Astropart. Phys.* **01**, 037 (2019), [arXiv:1805.09483\[astro-ph.CO\]](#).
- [172] S.-L. Cheng, W. Lee, and K.-W. Ng, *Superhorizon curvature perturbation in ultra-slow-roll inflation*, *Phys. Rev. D* **99**, 063524 (2019), [arXiv:1811.10108\[astro-ph.CO\]](#).

- [173] S. S. Mishra and V. Sahni, *Primordial Black Holes from a tiny bump/dip in the Inflaton potential*, J. Cosmol. Astropart. Phys. **04**, 007 (2020), [arXiv:1911.00057\[gr-qc\]](#).
- [174] H. V. Ragavendra, P. Saha, L. Sriramkumar and J. Silk, *PBHs and secondary GWs from ultra slow roll and punctuated inflation*, Phys. Rev. D **103**, 083510 (2021), [arXiv:2008.12202\[astro-ph.CO\]](#).
- [175] K. Kefala, G. P. Kodaxis, I. D. Stamou, and N. Tetradis, *Features of the inflaton potential and the power spectrum of cosmological perturbations*, Phys. Rev. D **104**, 023506 (2021), [arXiv:2010.12483\[astro-ph.CO\]](#).
- [176] Y.-P. Wu, E. Pinetti, K. Petraki, and J. Silk, *Baryogenesis from ultra-slow-roll inflation*, J. High Energy Phys. **01**, 015 (2022), [arXiv:2109.00118\[hep-ph\]](#).
- [177] O. Özsoy and G. Tasinato, *Consistency conditions and primordial black holes in single field inflation*, Phys. Rev. D **105**, 023524 (2022), [arXiv:2111.02432\[astro-ph.CO\]](#).
- [178] S. Hooshangi, A. Talebian, M. H. Namjoo, and H. Firouzjahi, *Multiple Field Ultra Slow Roll Inflation: Primordial Black Holes From Straight Bulk And Distorted Boundary*, Phys. Rev. D **105**, 083525 (2022), [arXiv:2201.07258\[astro-ph.CO\]](#).
- [179] G. Franciolini and A. Urbano, *Primordial black hole dark matter from inflation: the reverse engineering approach*, Phys. Rev. D **106**, 123519 (2022), [arXiv:2207.10056\[astro-ph.CO\]](#).
- [180] B.-M. Gu, F.-W. Shu, K. Yang, and Y.-P. Zhang, *Primordial black holes from an inflationary potential valley*, Phys. Rev. D **107**, 023519 (2023), [arXiv:2207.09968\[astro-ph.CO\]](#).
- [181] B. Mu, G. Cheng, J. Liu, and Z.-K. Guo, *Constraints on ultra-slow-roll inflation from the third LIGO-Virgo observing run*, Phys. Rev. D **107**, 043528 (2023), [arXiv:2211.05386\[astro-ph.CO\]](#).
- [182] B. Mu, J. Liu, G. Cheng, and Z.-K. Guo, *Constraints on ultra-slow-roll inflation with the NANOGrav 15-Year dataset*, J. Cosmol. Astropart. Phys. **11**, 065 (2024), [arXiv:2310.20564\[astro-ph.CO\]](#).
- [183] H. V. Ragavendra, A. K. Sarkar, and S. K. Sethi, *Constraining ultra slow roll inflation using cosmological datasets*, J. Cosmol. Astropart. Phys. **07**, 088 (2024), [arXiv:2404.00933\[astro-ph.CO\]](#).
- [184] J. Kristiano and J. Yokoyama, *Comparing sharp and smooth transitions of the second slow-roll parameter in single-field inflation*, J. Cosmol. Astropart. Phys. **10**, 036 (2024), [arXiv:2405.12145\[astro-ph.CO\]](#).
- [185] G. Autieri and M. Redi, *Reconstructing the inflaton potential: primordial black holes and gravitational waves in slow roll and ultra slow roll single field inflation*, J. Cosmol. Astropart. Phys. **01**, 154 (2025), [arXiv:2408.12587\[astro-ph.CO\]](#).
- [186] V. Aragam, S. Paban, and R. Rosati, *Primordial stochastic gravitational wave backgrounds from a sharp feature in three-field inflation. Part II. The inflationary era*, J. Cosmol. Astropart. Phys. **04**, 031 (2025), [arXiv:2409.09023\[astro-ph.CO\]](#).
- [187] S. Tripathy, D. Chowdhury, H. V. Ragavendra, and L. Sriramkumar, *Cross-correlation between the curvature perturbations and magnetic fields in pure ultra slow roll inflation*, Phys. Rev. D **111**, 063550 (2025), [arXiv:2409.20232\[astro-ph.CO\]](#).
- [188] J. Á. Ruiz and J. Rey, *Gravitational waves in ultra-slow-roll and their anisotropy at two loops*, J. Cosmol. Astropart. Phys. **04**, 026 (2025), [arXiv:2410.09014\[astro-ph.CO\]](#).
- [189] M. Cielo, G. Mangano, O. Pisanti, and D. Wands, *Steepest growth in the primordial power spectrum from excited states at a sudden transition*, J. Cosmol. Astropart. Phys. **04**, 007 (2025), [arXiv:2410.22154\[astro-ph.CO\]](#).

- [190] A. Caravano, G. Franciolini, and S. Renaux-Petel, *Ultra-Slow-Roll Inflation on the Lattice I: Backreaction and Nonlinear Effects*, Phys. Rev. D **111**, 6 (2025), [arXiv:2410.23942\[astro-ph.CO\]](#).
- [191] D. Sharma, *Stochastic inflation and non-perturbative power spectrum beyond slow roll*, J. Cosmol. Astropart. Phys. **03**, 017 (2025), [arXiv:2411.08854\[astro-ph.CO\]](#).
- [192] C.-J. Fang, Z.-H. Lyu, C. Chen, and Z.-K. Guo, *Incorporating Backreaction in One-Loop Corrections in Ultra-Slow-Roll Inflation*, [arXiv:2502.09555\[gr-qc\]](#).
- [193] Q. Wang, Y.-C. Liu, B.-Y. Su, and N. Li, *Primordial black holes from the perturbations in the inflaton potential in peak theory*, Phys. Rev. D **104**, 083546 (2021), [arXiv:2111.10028\[astro-ph.CO\]](#).
- [194] Y.-C. Liu, Q. Wang, B.-Y. Su, and N. Li, *Primordial black holes from the perturbations in the inflaton potential*, Phys. Dark Univ. **34**, 100905 (2021).
- [195] J.-X. Zhao, X.-H. Liu, and N. Li, *Primordial black holes and scalar-induced gravitational waves from the perturbations on the inflaton potential in peak theory*, Phys. Rev. D **107**, 043515 (2023), [arXiv:2302.06886\[astro-ph.CO\]](#).
- [196] H.-R. Zhao, Y.-C. Liu, J.-X. Zhao, and N. Li, *The evolution of the primordial curvature perturbation in the ultraslow-roll inflation*, Eur. Phys. J. C **83**, 783 (2023).
- [197] J.-X. Zhao and N. Li, *An analytical approximation of the evolution of the primordial curvature perturbation in the ultraslow-roll inflation*, Eur. Phys. J. C **84**, 222 (2024), [arXiv:2403.01416\[astro-ph.CO\]](#).
- [198] B.-Y. Su, N. Li, and L. Feng, *Primordial black holes from the ultraslow-roll phase in the inflaton-curvaton mixed field inflation*, Eur. Phys. J. C **85**, 197 (2025), [arXiv:2502.14323\[astro-ph.CO\]](#).
- [199] L. T. Witkowski, *SIGWfast: a python package for the computation of scalar-induced gravitational wave spectra*, [arXiv:2209.05296\[astro-ph.CO\]](#)
- [200] E. Thrane and C. Talbot, *An introduction to Bayesian inference in gravitational-wave astronomy: parameter estimation, model selection, and hierarchical models*, Publ. Astron. Soc. Austral. **36**, e010 (2019), [arXiv:1809.02293\[astro-ph.IM\]](#).
- [201] A. Mitridate, D. Wright, R. von Eckardstein, T. Schröder, J. Nay, K. Olum, K. Schmitz, and T. Trickle, *PTArcade*, [arXiv:2306.16377\[hep-ph\]](#).
- [202] J. E. Gammal *et al.* [LISA Cosmology Working Group], *Reconstructing Primordial Curvature Perturbations via Scalar-Induced Gravitational Waves with LISA*, [arXiv:2501.11320\[astro-ph.CO\]](#).
- [203] M. Sasaki, *Gauge-Invariant Scalar Perturbations in the New Inflationary Universe*, Prog. Theor. Phys. **70**, 394 (1983).
- [204] V. F. Mukhanov, *Quantum theory of gauge-invariant cosmological perturbations*, Sov. Phys. JETP **68**, 1297 (1988).
- [205] S. Kachru, R. Kallosh, A. Linde, and S. P. Trivedi, *de Sitter Vacua in String Theory*, Phys. Rev. D **68**, 046005 (2003), [arXiv:0301240\[hep-th\]](#).
- [206] A. A. Starobinsky, *A New Type of Isotropic Cosmological Models Without Singularity*, Phys. Lett. B **91**, 99 (1980).
- [207] A. M. Green, A. R. Liddle, K. A. Malik, and M. Sasaki, *A new calculation of the mass fraction of primordial black holes*, Phys. Rev. D **70**, 041502 (2004), [arXiv:0403181\[astro-ph\]](#).
- [208] J. M. Bardeen, J. R. Bond, N. Kaiser, and A. S. Szalay, *The Statistics of Peaks of Gaussian Random Fields*, Astrophys. J. **304**, 15 (1986).



- [209] I. Musco, *Threshold for primordial black holes: Dependence on the shape of the cosmological perturbations*, Phys. Rev. D **100**, 123524 (2019), [arXiv:1809.02127\[gr-qc\]](#).
- [210] I. Musco, J. C. Miller and L. Rezzolla, *Computations of primordial black hole formation*, Class. Quant. Grav. **22**, 1405 (2005), [arXiv:0412063\[gr-qc\]](#).
- [211] T. Harada, C. M. Yoo, and K. Kohri, *Threshold of primordial black hole formation*, Phys. Rev. D **88**, 084051 (2013), [arXiv:1309.4201\[astro-ph.CO\]](#).
- [212] T. Nakama, T. Harada, A. G. Polnarev and J. Yokoyama, *Identifying the most crucial parameters of the initial curvature profile for primordial black hole formation*, J. Cosmol. Astropart. Phys. **01**, 037 (2014), [arXiv:1310.3007\[gr-qc\]](#).
- [213] A. Escrivà, *Simulation of primordial black hole formation using pseudo-spectral methods*, Phys. Dark Univ. **27**, 100466 (2020), [arXiv:1907.13065\[gr-qc\]](#).
- [214] I. Musco, V. De Luca, G. Franciolini, and A. Riotto, *Threshold for primordial black holes. II. A simple analytic prescription*, Phys. Rev. D **103**, 063538 (2021), [arXiv:2011.03014\[astro-ph.CO\]](#).
- [215] I. Musco and T. Papanikolaou, *Primordial black hole formation for an anisotropic perfect fluid: Initial conditions and estimation of the threshold*, Phys. Rev. D **106**, 083017 (2022), [arXiv:2110.05982\[gr-qc\]](#).
- [216] T. Papanikolaou, *Toward the primordial black hole formation threshold in a time-dependent equation-of-state background*, Phys. Rev. D **105**, 124055 (2022), [arXiv:2205.07748\[gr-qc\]](#).
- [217] I. D. Stamou, *Exploring critical overdensity thresholds in inflationary models of primordial black holes formation*, Phys. Rev. D **108**, 063515 (2023), [arXiv:2306.02758\[astro-ph.CO\]](#).
- [218] G. Domènech, *Scalar induced gravitational waves review*, Universe **7**, 398 (2021), [arXiv:2109.01398\[gr-qc\]](#).
- [219] R. A. Isaacson, *Gravitational Radiation in the Limit of High Frequency. I. The Linear Approximation and Geometrical Optics*, Phys. Rev. **166**, 1263 (1968).
- [220] R. A. Isaacson, *Gravitational Radiation in the Limit of High Frequency. II. Nonlinear Terms and the Effective Stress Tensor*, Phys. Rev. **166**, 1272 (1968).
- [221] K. N. Ananda, C. Clarkson, and D. Wands, *The cosmological gravitational wave background from primordial density perturbations*, Phys. Rev. D **75**, 123518 (2007), [arXiv:0612013\[gr-qc\]](#).
- [222] W.-T. Xu, J. Liu, T.-J. Gao, and Z.-K. Guo, *Low-frequency Gravitational Waves from Double-inflection-point Inflation*, Phys. Rev. D **101**, 023505 (2020), [arXiv:1907.05213\[astro-ph.CO\]](#).
- [223] K. Saikawa and S. Shirai, *Precise WIMP Dark Matter Abundance and Standard Model Thermodynamics*, J. Cosmol. Astropart. Phys. **08**, 011 (2020), [arXiv:2005.03544\[hep-ph\]](#).
- [224] D. Croon, D. McKeen, and N. Raj, *Gravitational microlensing by dark matter in extended structures*, Phys. Rev. D **101**, 083013 (2020), [arXiv:2002.08962\[astro-ph.CO\]](#).
- [225] H. Niikura, M. Takada, S. Yokoyama, T. Sumi, and S. Masaki, *Gravitational microlensing by dark matter in extended structures*, Phys. Rev. D **99**, 083503 (2019), [arXiv:1901.07120\[astro-ph.CO\]](#).
- [226] V. Atal and G. Domènech, *Probing non-Gaussianities with the high frequency tail of induced gravitational waves*, J. Cosmol. Astropart. Phys. **06**, 001 (2021), [arXiv:2103.01056\[astro-ph.CO\]](#).
- [227] G. Ferrante, G. Franciolini, A. Iovino, Junior., and A. Urbano, *Primordial non-Gaussianity up to all orders: Theoretical aspects and implications for primordial black hole models*, Phys. Rev. D **107**, 043520 (2023), [arXiv:2211.01728\[astro-ph.CO\]](#).

- [228] S. Wang, Z.-C. Zhao, J.-P. Li, and Q.-H. Zhu, *Implications of pulsar timing array data for scalar-induced gravitational waves and primordial black holes: Primordial non-Gaussianity  $f_{\text{NL}}$  considered*, Phys. Rev. Res. **6**, L012060 (2024), [arXiv:2307.00572\[astro-ph.CO\]](#).
- [229] L. Liu, Z.-C. Chen, and Q.-G. Huang, *Implications for the non-Gaussianity of curvature perturbation from pulsar timing arrays*, Phys. Rev. D **109**, 6 (2024), [arXiv:2307.01102\[astro-ph.CO\]](#).
- [230] S. Choudhury, K. Dey, A. Karde, S. Panda, and M. Sami, *Primordial non-Gaussianity as a saviour for PBH overproduction in SIGWs generated by pulsar timing arrays for Galileon inflation*, Phys. Lett. B **856**, 138925 (2024), [arXiv:2310.11034\[astro-ph.CO\]](#).
- [231] S. Choudhury, K. Dey, S. Ganguly, A. Karde, S. K. Singh, and P. Tiwari, *Negative non-Gaussianity as a salvager for PBHs with PTAs in bounce*, Eur. Phys. J. C **85**, 472 (2025), [arXiv:2409.18983\[astro-ph.CO\]](#).
- [232] R. Inui, C. Joana, H. Motohashi, S. Pi, Y. Tada, and S. Yokoyama, *Primordial black holes and induced gravitational waves from logarithmic non-Gaussianity*, J. Cosmol. Astropart. Phys. **03**, 021 (2025), [arXiv:2411.07647\[astro-ph.CO\]](#).
- [233] K. Inomata, K. Kohri, and T. Terada, *Detected stochastic gravitational waves and subsolar-mass primordial black holes*, Phys. Rev. D **109**, 063506 (2024), [arXiv:2306.17834\[astro-ph.CO\]](#).
- [234] X. Wang, X.-H. Ma, and Y.-F. Cai, *Primordial black hole formation from the upward step model: Avoiding overproduction*, Int. J. Mod. Phys. D **34**, 2550027 (2025), [arXiv:2412.19631\[astro-ph.CO\]](#).
- [235] K. Harigaya, K. Inomata, and T. Terada, *Induced gravitational waves with kination era for recent pulsar timing array signals*, Phys. Rev. D **108**, 123538 (2023), [arXiv:2309.00228\[astro-ph.CO\]](#).
- [236] C. Unal, A. Papageorgiou, and I. Obata, *Axion-gauge dynamics during inflation as the origin of pulsar timing array signals and primordial black holes*, Phys. Lett. B **856**, 138873 (2024), [arXiv:2307.02322\[astro-ph.CO\]](#).
- [237] S. Pi, M. Sasaki, V. Takhistov, and J. Wang, *Primordial Black Hole Formation from Power Spectrum with Finite-width*, [arXiv:2501.00295\[astro-ph.CO\]](#).
- [238] G. Ferrante, G. Franciolini, A. Iovino, Junior., and A. Urbano, *Primordial black holes in the curvaton model: possible connections to pulsar timing arrays and dark matter*, J. Cosmol. Astropart. Phys. **06**, 057 (2023), [arXiv:2305.13382\[astro-ph.CO\]](#).
- [239] A. D. Gow, T. Miranda, and S. Nurmi, *Primordial black holes from a curvaton scenario with strongly non-Gaussian perturbations*, J. Cosmol. Astropart. Phys. **11**, 006 (2023), [arXiv:2307.03078\[astro-ph.CO\]](#).
- [240] M. A. Gorji, M. Sasaki, and T. Suyama, *Extra-tensor-induced origin for the PTA signal: No primordial black hole production*, Phys. Lett. B **846**, 138214 (2023), [arXiv:2307.13109\[astro-ph.CO\]](#).
- [241] S. Choudhury, A. Karde, S. Panda, and M. Sami, *Realisation of the ultra-slow roll phase in Galileon inflation and PBH overproduction*, J. Cosmol. Astropart. Phys. **07**, 034 (2024), [arXiv:2401.10925\[astro-ph.CO\]](#).
- [242] A. Afzal and A. Ghoshal, *Primordial black holes and scalar-induced gravitational waves in radiative hybrid inflation*, Eur. Phys. J. C **84**, 983 (2024), [arXiv:2402.06613\[astro-ph.CO\]](#).
- [243] S. Choudhury, S. Ganguly, S. Panda, S. SenGupta, and P. Tiwari, *Obviating PBH overproduction for SIGWs generated by pulsar timing arrays in loop corrected EFT of bounce*, J. Cosmol. Astropart. Phys. **09**, 013 (2024), [arXiv:2407.18976\[astro-ph.CO\]](#).

- [244] C. T. Byrnes, P. S. Cole, and S. P. Patil, *Steepest growth of the power spectrum and primordial black holes*, J. Cosmol. Astropart. Phys. **06**, 028 (2019), [arXiv:1811.11158\[astro-ph.CO\]](#).
- [245] J. Liu, Z.-K. Guo, and R.-G. Cai, *Analytical approximation of the scalar spectrum in the ultra-slow-roll inflationary models*, Phys. Rev. D **101**, 083535 (2020), [arXiv:2003.02075\[astro-ph.CO\]](#).
- [246] G. H. Janssen *et al.*, *Gravitational wave astronomy with the SKA*, Proceedings of Science **AASKA14**, 037 (2015), [arXiv:1501.00127\[astro-ph.IM\]](#).
- [247] P. Amaro-Seoane *et al.* [LISA], *Laser Interferometer Space Antenna*, [arXiv:1702.00786\[astro-ph.IM\]](#).
- [248] V. Corbin and N. J. Cornish, *Detecting the Cosmic Gravitational Wave Background with the Big Bang Observer*, Class. Quant. Grav. **23**, 2435 (2006), [arXiv:0512039\[gr-qc\]](#).
- [249] S. Babak, M. Falxa, G. Franciolini, and M. Pieroni, *Forecasting the sensitivity of pulsar timing arrays to gravitational wave backgrounds*, Phys. Rev. D **110**, 063022 (2024), [arXiv:2404.02864\[astro-ph.CO\]](#).
- [250] M. Rajagopal and R. W. Romani, *Ultra-Low Frequency Gravitational Radiation from Massive Black Hole Binaries*, Astrophys. J. **446**, 543 (1995), [arXiv:9412038\[astro-ph\]](#).
- [251] A. H. Jaffe and D. C. Backer, *Gravitational Waves Probe the Coalescence Rate of Massive Black Hole Binaries*, Astrophys. J. **583**, 616 (2003), [arXiv:0210148\[astro-ph\]](#).
- [252] S. Burke-Spolaor *et al.*, *The Astrophysics of Nanohertz Gravitational Waves*, Astron. Astrophys. Rev. **27**, 5 (2019), [arXiv:1811.08826\[astro-ph.HE\]](#).